R-08-129

NDT Reliability – Final Report

Reliability in non-destructive testing (NDT) of the canister components

Mato Pavlovic, Kazunori Takahashi,
Christina Müller, Rainer Boehm,
BAM – Federal Institute for Materials
Research and Testing, Berlin

Ulf Ronneteg, Svensk Kärnbränslehantering AB

December 2008

Svensk Kärnbränslehantering AB
Swedish Nuclear Fuel
and Waste Management Co

Box 250, SE-101 24 Stockholm
Phone +46 8 459 84 00

ISSN 1402-3091
SKB Rapport R-08-129

NDT Reliability – Final Report

Reliability in non-destructive testing (NDT) of the canister components

Mato Pavlovic, Kazunori Takahashi,
Christina Müller, Rainer Boehm,
BAM – Federal Institute for Materials
Research and Testing, Berlin

Ulf Ronneteg, Svensk Kärnbränslehantering AB

December 2008

Abstract

This report describes the methodology of the reliability investigation performed on the ultrasonic phased array NDT system, developed by SKB in collaboration with Posiva, for inspection of the canisters for permanent storage of nuclear spent fuel.

The canister is composed of a cast iron insert surrounded by a copper shell. The shell is composed of the tube and the lid/base which are welded to the tube after the fuel has been place, in the tube. The manufacturing process of the canister parts and the welding process are described. Possible defects, which might arise in the canister components during the manufacturing or in the weld during the welding, are indentified.

The number of real defects in manufactured components have been limited. Therefore the reliability of the NDT system has been determined using a number of test objects with artifical defects.

The reliability analysis is based on the signal response analysis. The conventional signal response analysis is adopted and further developed before applied on the modern ultrasonic phased-array NDT system. The concept of multi-parameter a, where the response of the NDT system is dependent on more than just one parameter, is introduced. The weakness of use of the peak signal response in the analysis is demonstrated and integration of the amplitudes in the C-scan is proposed as an alternative. The calculation of the volume POD, when the part is inspected with more configurations, is also presented. The reliability analysis is supported by the ultrasonic simulation based on the point source synthesis method.

Contents

1	**Introduction**	7
1.1	Background	7
1.1.1	Nuclear spent fuel	7
1.1.2	KBS-3 method	7
1.1.3	Canister	7
1.1.4	NDT of the canister	9
1.1.5	Reliability	9
1.2	Strategy	10
1.3	Structure of the report	12
2	**Canister components**	13
2.1	Copper tube	13
2.1.1	Extrusion process	13
2.1.2	Possible defects in copper tube	15
2.2	Copper lid/base	15
2.2.1	Forging process	15
2.2.2	Possible defects in copper lid/base	15
2.3	Cast iron insert	16
2.3.1	Casting process	16
2.3.2	Possible defects in the cast iron insert	18
2.4	Welding of the lid/base and the tube	19
2.4.1	Welding process	19
2.4.2	Possible defects in the weld	20
3	**Non-destructive testing by ultrasound**	21
3.1	General	21
3.2	NDT for copper tube	21
3.2.1	NDT system for copper tube	21
3.2.2	NDT processes for copper tube	22
3.2.3	Test objects for copper tube	22
3.3	NDT for copper lid/base	23
3.3.1	NDT system for the copper lid/base	23
3.3.2	NDT processes for copper lid/base	24
3.3.3	Test objects for copper lid/base	24
3.4	NDT for cast iron insert	25
3.4.1	NDT system for cast iron insert	25
3.4.2	NDT processes for cast iron insert	25
3.4.3	Test objects for cast iron insert	27
3.5	NDT for friction stir welding (FSW)	27
3.5.1	NDT system for FSW	28
3.5.2	NDT processes for the FSW	28
4	**Modelling**	29
4.1	Principles of modelling	29
4.2	Simulation software	30
5	**Reliability analysis**	33
5.1	Conventional POD analysis	33
5.1.1	$\hat{a}$ versus a analysis	33
5.1.2	Calculation of the POD	34
5.1.3	95% Confidence bounds	35

5.2 The POD I analysis 36
5.2.1 Multi-parameter *a* 36
5.2.2 The POD of the flaw in the volume 40
5.3 The POD II analysis 46
5.3.1 Methodology 47
5.3.2 Application and results of the method 49

6 Conclusions 53
6.1 Conclusions from the POD I analysis 53
6.2 Conclusions from the POD II analysis 54
6.3 ENIQ considerations 54

7 References 55

1 Introduction

In the introductory chapter a short background of the problem of nuclear waste handling, together with the strategy of the project "NDT Reliability" project is presented, followed by the structure of the report.

1.1 Background

The nuclear power industry has the responsibility for management and disposal of all radioactive waste from its plants. Because of the unique treatment of nuclear spent fuel, special system for disposal has to be developed.

1.1.1 Nuclear spent fuel

Generation of electricity in nuclear power plants, like in all thermal power plants, produces spent nuclear fuel. Because the large amount of energy that is available from small amount of spent fuel, the amount of spent fuel is also small. However, this is radioactive and dangerous for man and the environment and needs to be carefully managed. Delay-and-decay principle is unique to radioactive waste management; it means that the waste is stored and its radioactivity is allowed to decrease naturally through decay of the radioisotopes in it.

1.1.2 KBS-3 method

The method to manage nuclear spent fuel being investigated by SKB and Posiva is called KBS-3 method, described in /1/ and evaluated in terms of its long-term safety in /2/. It calls for the spent nuclear fuel to be encapsulated in copper. The copper canisters will be deposited in the bedrock, embedded in clay, at a depth of about 500 metres. When deposition is finished the tunnels and rock caverns will be sealed.

The fuel will be taken from the interim storage facility for spent nuclear fuel, where it has been stored for 30–40 years, and placed in leak tight copper canisters with a cast iron insert. The canisters will then be transported down to a deep repository consisting of a system of horizontal tunnels at a depth of 400–700 metres in the bedrock.

The tunnels will be about 250 metres long and spaced at a distance of about 40 metres from each other. On the floor of the tunnels, deposition holes will be spaced at intervals of about 6 metres. The copper canisters will be deposited in the deposition holes and surrounded by a buffer of bentonite. When deposition is finished, the tunnels and shafts will be back-filled. The method is schematically illustrated in Figure 1-1.

1.1.3 Canister

The canister is approximately five metres long and has a diameter of over one meter. The shell is made of copper due to its high resistance to corrosion. It is five centimetres thick and should prevent contact of the content of the canister with the environment. Inner part made of cast iron is designed to withstand mechanical loads imposed on the canister.

The parts of the canister are copper tube, lid and base which make outer shell and insert made of nodular cast iron. The lid and the base are welded to the tube to seal the canister. Filled with spent nuclear fuel, canister weighs between 25 and 27 tonnes. The canister is shown schematically in Figure 1-2.

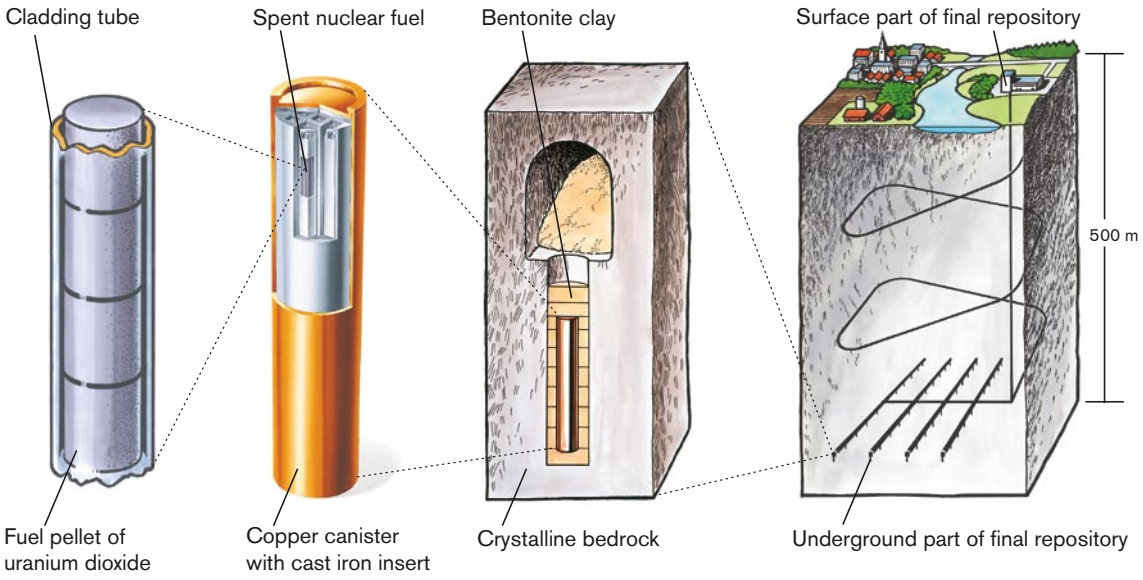

Figure 1-1. *KBS-3 method for deposit of the spent nuclear fuel.*

5 cm copper

Estimated weight (kg):

Copper canister	7,400
Insert	13,600
Fuel assembly (BWR)	3,600
Totalt	24,600

Figure 1-2. *Canister for storage of spent nuclear fuel.*

1.1.4 NDT of the canister

The field of Non-destructive Testing (NDT) is a very broad, interdisciplinary field that plays a critical role in assuring that structural components and systems perform their function. These tests are performed in a manner that does not affect the future usefulness of the object or material. In other words, with NDT components and material are inspected and measured without damaging them. NDT is performed on all parts of the canister and on the welds to ensure that no critical defect is present. From many different available NDT methods, the advanced ultrasonic (UT) phased array system is selected as a primary method for the inspection. Schematic view of the inspection of the copper tube is shown in Figure 1-3.

1.1.5 Reliability

Inspection systems, even the most advanced, when applied at the extreme of capability for finding small defects, will not detect all defects of the same size. It is known from the practice that even repeated inspections of the same defect will not always detect it, meaning that the measurements are not consistent due to the noise, measurement errors, inconsistency of setups. This is why we introduce the concept of reliability.

The technical definition of reliability is the probability that a system or a device will perform its intended function under operating conditions. In our case, the system is the NDT system and its function is to detect a defect. Performing the reliability analysis we estimate the probability with which the NDT system will find a defect of certain properties (type, size, orientation, depth).

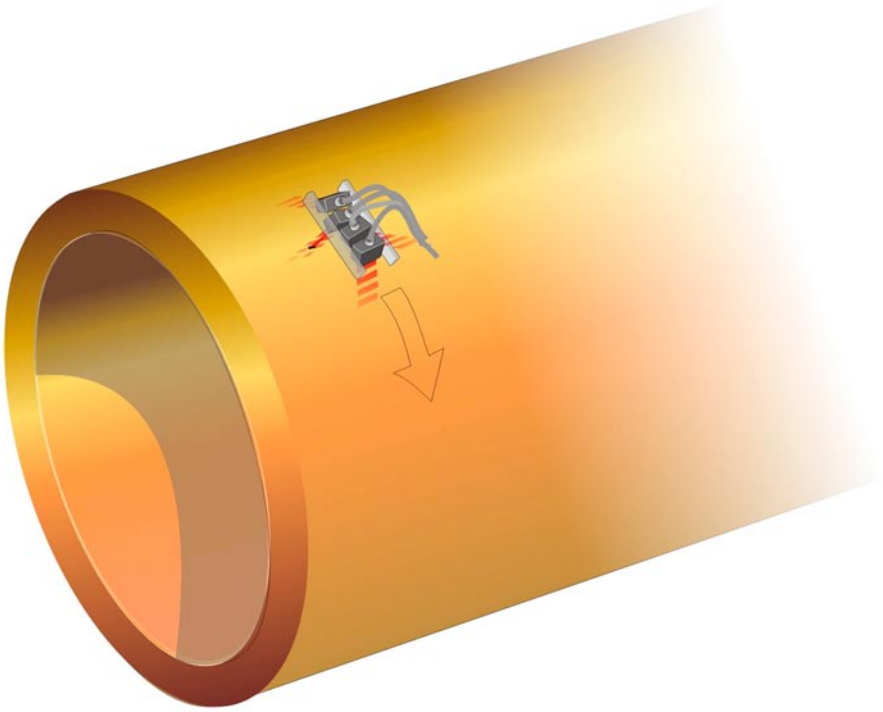

Figure 1-3. *Ultrasonic inspection of copper tube.*

An important aspect of the reliability analysis is the NDT experiment. Evaluating the data from the experiment we establish the capability of the NDT system in terms of a representative POD curve and its lower confidence bound. The POD curve gives us an estimation of the reliability of the system and the lower confidence bound gives us a measure of confidence in our estimation.

To accept the NDT system for a given task we need to set the acceptance criteria. Our estimation of the reliability of the system should guarantee that the critical flaw will be detected with 90% probability and 95% confidence. That means that in the POD diagram the critical defect will be larger than the $a_{90/95}$ value.

1.2 Strategy

The "Non-Destructive Testing Reliability Project" is a joint project between Swedish Nuclear Fuel and Waste management Co (Svensk Kärnbränslehantering AB, SKB); Posiva, a Finnish expert organisation responsible for the final disposal of spent nuclear fuel and German Federal Institute for Material Research and Testing (Bundesanstalt für Materialforschung und – prüfung, BAM). The project is a subpart of the total risk assessment of the final repository.

The canisters in which the spent nuclear fuel will be stored have to ensure that the content will not come in contact with the environment for a long period of time. During the manufacturing process of components of the canister and during the welding of the lid/base to the tube, defects might occur in the material. These defects might jeopardize the function of the canisters. To ensure the required quality of the parts and the weld, NDT inspection is performed after the manufacturing of the components and after the welding process. The aim of the project is to determine the reliability of NDT techniques used for inspections.

SKB has built Canister Laboratory where both the encapsulation technique and the NDT are performed on full-scale objects. The advantage of working with real size objects is that geometrical influences are incorporated in the results from the very beginning of the development of the NDT system. The influence of modules of the system on the total reliability (for example influence of fixtures for probes and manipulators) is included in the reliability analysis already in the early optimisation phase of the development of the system. These modules have important influence on the total reliability of the NDT system.

For a successful reliability study, a statistically significant number of defects has to be evaluated. The best, most realistic way is to test the system against the real defects, ones that occur naturally during the manufacturing process. Since these occur rarely, they are generally available only for objects which are long time in production. The production of the canister parts has been started only recently, so no such defects are available. To overcome this problem, the plan is to manipulate parameters of the manufacturing process, forcing occurrence of the so called realistic defects. So far, only a few defects were created in this way. Once the objects with defects are inspected with the NDT system, the real geometry of the defect has to be known for reliability analysis. The destructive testing, cutting the object slice by slice while taking photographs of individual slices, makes reconstruction of the flaw possible.

Another method, often used when testing NDT systems is to produce flaws artificially. These flaws are usually in the form of a flat-bottom hole (FBH), side-drilled hole (SDH) and notch. The advantage of these defects is that they can be produced in various sizes, orientations and depths, creating large sample for statistical analysis. Their relatively simple geometrical shape also allows model simulation of their response to the NDT system.

To reduce the number of artificially produced defects, the response to the NDT system is simulated with the BAM simulation software. The simulation reduces the costs of manufacturing of defects in a wide range of sizes, depths and orientations.

As guidelines for reliability analysis, recommendations from US Department of Defence Handbook MIL 1823 /4/ as well as European methodology for qualification of non-destructive tests /5/ have been followed. MIL 1823 provides uniform guidance requirements for establishing NDT procedures used to inspect new or in-service hardware for which a measure of NDT reliability is required. ENIQ document sets out the principles that a body carrying out qualification of NDT should follow in providing certification that a given test is fit for its purpose. In addition, number of literature that explains the theoretical background of the reliability analysis are available, e.g. /6/. In the former project, the reliability analysis proposed in those documents is simply applied to radiography and ultrasonic testing results /7/, /8/. However, because of the complicated interaction of the advanced ultrasonic phased array NDT system and the defect, it is necessary to modify and further develop procedures recommended in these documents.

In conventional POD calculation with the $\hat{a}$ versus a approach, it is common to take defect size as a and echo height from the defect as $\hat{a}$. The analysis was originally developed for eddy current testing, where very clear linear relationship between defect size (length) and the response can be observed. This definition has been also applied and widely used for ultrasonic testing of thin objects, especially in aerospace industry, where defect size is most dominant factor of the response. However, in the case of inspection of canisters, the maximum inspection depth is more than 200 mm. In the deeper region of material, many parameters influence the response. Thus the echo height (amplitude) cannot be sufficiently expressed by a function of only the size of defects. This problem is clearly seen in the $\hat{a}$ versus a diagram, when the conventional definitions are applied. Measurement points are widely spread in the diagram, and linear relationship between echo height and defect size cannot be observed. Although points are scattered, POD curve can technically be calculated if there is enough number of samples. However, the confidence bound may be wider, meaning the analysis is inaccurate. In order to achieve narrower confidence bound and to analyse accurately, the method needs to be modified specifically for ultrasonic phased array measurements.

The problem in the conventional method seems to be in the assumption of the linear relationship between echo height $\hat{a}$ and size a. In the project, two approaches are developed which modify the definitions of a and $\hat{a}$, not the linear relationship itself.

The first approach intends to include not only size but also some other factors into a. As explained above, response (echo height, amplitude) of defect to phased array ultrasonic system is dependent on many factors. The size of defects may be most dominant one, but some other factors also have relatively larger influences and are not negligible, especially in deeper region. To include influences of several parameters, a is defined as the signal response of a defect predicted from its characteristics, called *multi-parameter a*. If the prediction is good enough, a should have a linear relationship to measured signal response $\hat{a}$ with a normally distributed deviation given by noise and the experimental errors. From this relationship the POD as a function of the multi-parameter a can be calculated the same way as in the conventional method. The POD can be devided into individual factors, which are included in the multi-parameter a. The analysis allows investigation of the influences of the individual factor on POD. In the development, defect size (diameter of FBH), depth (based on the sound-field) and orientation (tilt angle) are taken as parameters of multi-parameter a. The predicted amplitudes from those properties and also from other implicit factors are calculated with support of modelling.

In addition, a way of combining POD's given by several measurements for the same body is developed. The method, *volume POD*, can display the total POD of a defect and can display distribution of the total POD overlaying the geometry of the test body, which is an easy way to interpret the results.

The second approach is a modification of the definition of $\hat{a}$. The highest amplitude has been taken as $\hat{a}$ in the conventional analysis, and thus it is necessary to select a value for a defect. Depending on the shape or surface roughness of a defect, for example, the defect may give several local maxima. It is possible to select the global maximum as $\hat{a}$, but it may not represent the characteristics of the flaw any more. Moreover, only one amplitude value can easily be influenced by noise and measurement errors, meaning it is not robust. The basic idea of the development is to analyse reliability of a NDT system with complicated defects more robust by using more information than only one amplitude. In this approach, the new definition of $\hat{a}$ is introduced, which is integration of amplitude over defect area. The definition allows $\hat{a}$ to include a part of spatial information. When calculating the POD with the new definition of $\hat{a}$, the conventional way of threshold cannot be applied, and the new thresholding is proposed.

In the project as well as in this report, the first approach is called *POD I* analysis and the second *POD II* analysis.

1.3 Structure of the report

The report is structured as follows: in the next chapter the components of the canister are described, the manufacturing process and types of possible discontinuities which might occur during the process. In Chapter 3 the ultrasonic phased array NDT system used to inspect the components is described. In Chapter 4 the basics of modelling, which is used in the POD calculation, is explained, while Chapter 5 gives overview of the concept of reliability and POD, conventional approach and modification of the method for ultrasonic phased array inspection. Furthermore, application examples of the new developments to measurements with artificial defects are shown. Finally, in Chapter 6, conclusions are made from our work and some views how to proceed with the project are presented.

The report presents the general ideas, methodologies and application examples of the reliability analyses developed in the project. The results of the analyses and investigations on reliability of the ultrasonic NDT system for each component of the canister can be found in corresponding data reports, for the copper components /9/ and for the cast iron insert /10/.

2 Canister components

The canister consists of four components: the tube, the lid and the base made of copper and the insert made of nodular cast iron. During the manufacturing process defects might occur in these parts. Depending on their size, location and type, defects can jeopardize the function of the canister. No canister with the critical defect should be used for the storage. In order to ensure that no such defect is present, components are inspected with NDT. The material properties and geometrical features of components present different challenges for the NDT inspection.

Additionally, the weld between the lid/base and the tube is also inspected with NDT.

2.1 Copper tube

SKB and Posiva are simultaneosly developing technique for manufacturing of copper tubes by using three different methods; extrusion, pierce and draw technique and forging. SKB has chosed extrusion as the reference method for tube manufacturing and therefore only this type is handled in this report.

2.1.1 Extrusion process

The copper tube is manufactured from a heated ingot that is placed upright in a press, where it is compressed to a shorter length and a larger diameter. A hole is then made straight through the centre with a mandrel. The result is a relatively short tubular work-piece as shown in Figure 2-1. This hollow cylinder is then placed in the extrusion press and extruded in one step to its final size, as illustrated schematically in Figure 2-2. After cooling, the tube is pre-machined prior to the non-destructive testing. At this stage the tube has a copper thickness of 54 mm compared to the final thickness of 50 mm, see Figure 2-3.

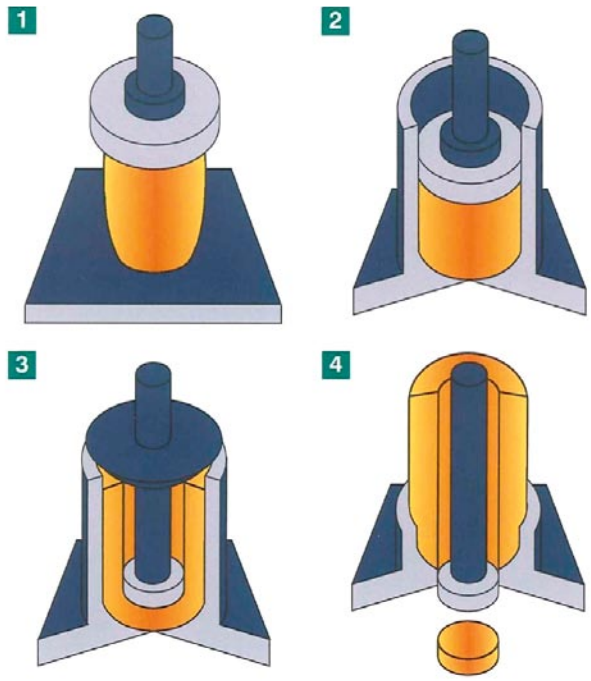

Figure 2-1. *Extrusion of copper tube, step 1.*

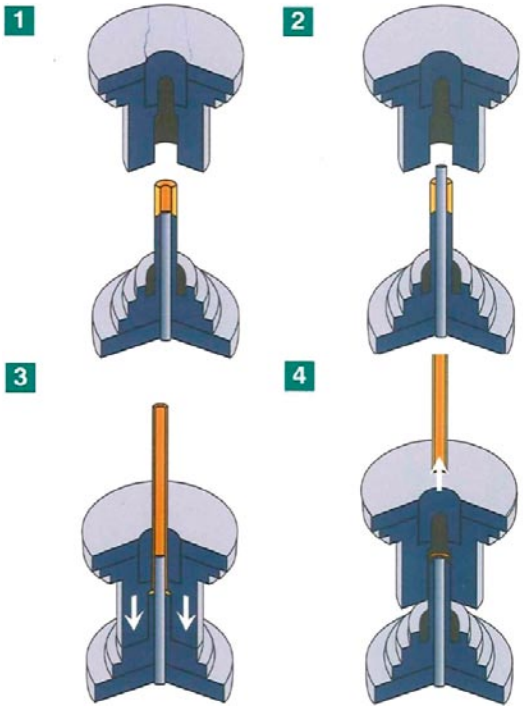

Figure 2-2. *Extrusion of copper tube, step 2.*

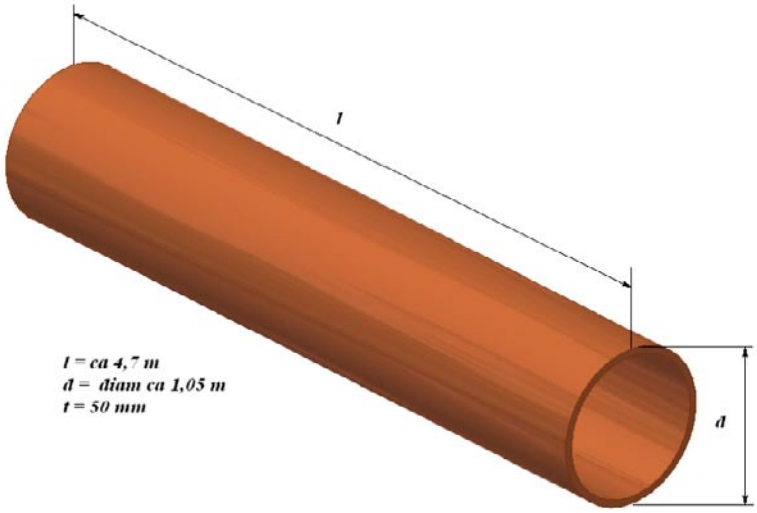

Figure 2-3. *General design of copper tube.*

2.1.2 Possible defects in copper tube

The possible discontinuities that have been identified in the copper tube are summarized in Table 2-1 below.

2.2 Copper lid/base

Copper lids and bases (see Figure 2-4) are made by forging of continuous-cast ingots.

2.2.1 Forging process

The forging process that using billets heated to ~700 ºC is described in Figure 2-5. The lid and base have individual design, however the pre-machined stage prior to the NDT are the same.

2.2.2 Possible defects in copper lid/base

The possible discontinuities that have been identified in the copper lid/base are summarized in Table 2-2 below.

Table 2-1. Possible defect types in copper tube.

Defect type	Comment
Inclusions	Clouds or stringers of oxide or foreign material with axial propagation.
Surface scratches	Axial scratches coming from irregularities in the surface of the extrusion press.

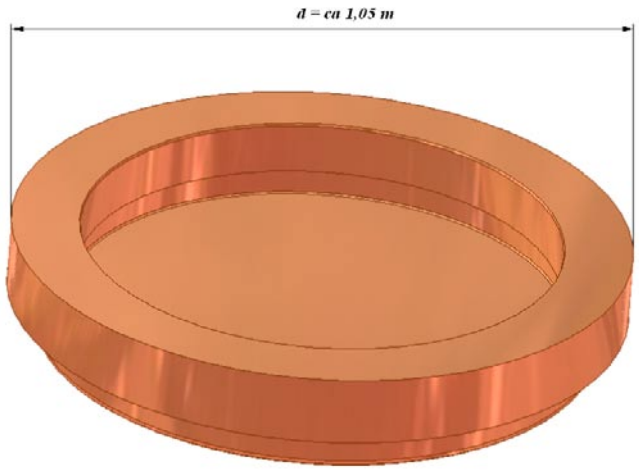

Figure 2-4. *General design of copper lid.*

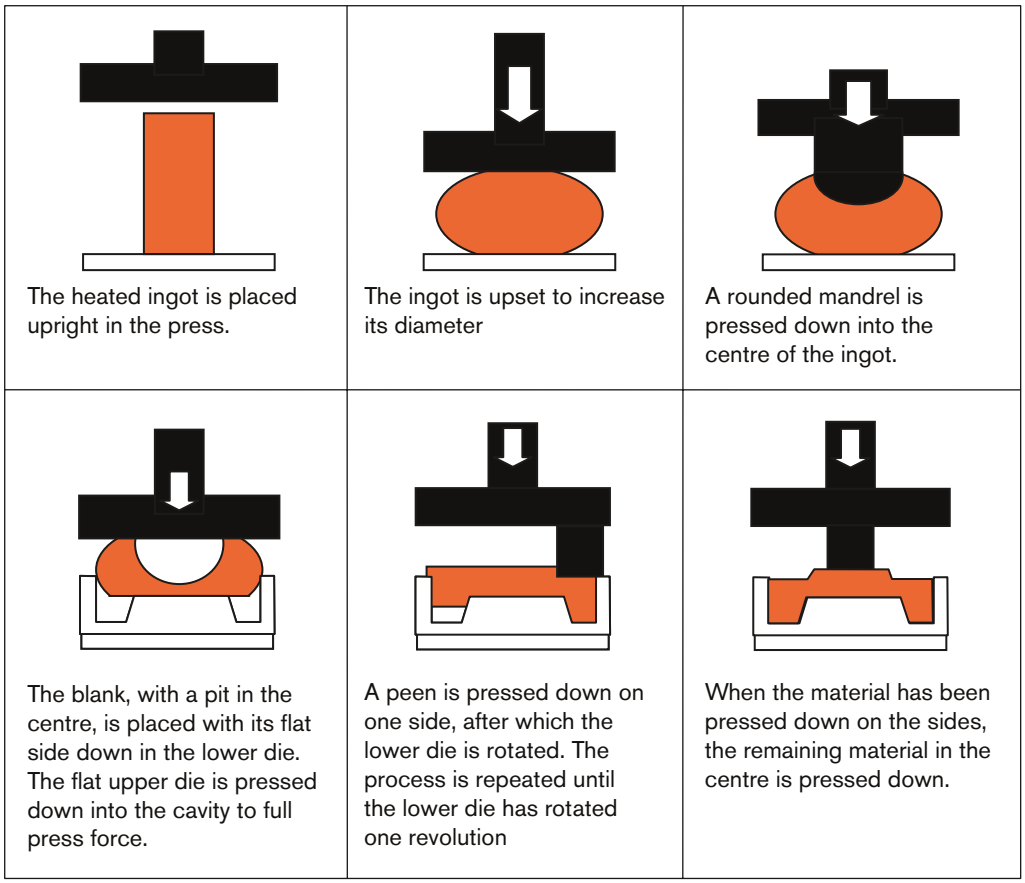

Figure 2-5. *Forging process of copper lid and base.*

Table 2-2. Possible defect types in copper lid and base.

Defect Type	Comment
Inclusions	Clouds or stringers of oxide or foreign material.
Laminations	From rolling over of edges.

2.3 Cast iron insert

Two types of inserts (see Figure 2-6) are manufactured by SKB[1]; one for the fuel from the boiling water reactors (BWR) and one for the pressure water reactors (PWR).

2.3.1 Casting process

The insert is manufactured from a nodular cast iron. First the steel cassette, see Figure 2-7, is placed in the mould and the square tubes are filled with packed sand. Then the mould is filled with molten iron either from top (see Figure 2-8) or from the bottom depending on the manufacturer. After cooling, the insert is knocked out of the mould and pre-machined prior to the non-destructive testing. At this stage the insert has an extra thickness of ~5 mm compared to the finally machined insert (Figure 2-9).

[1] Posiva has one additional type of insert.

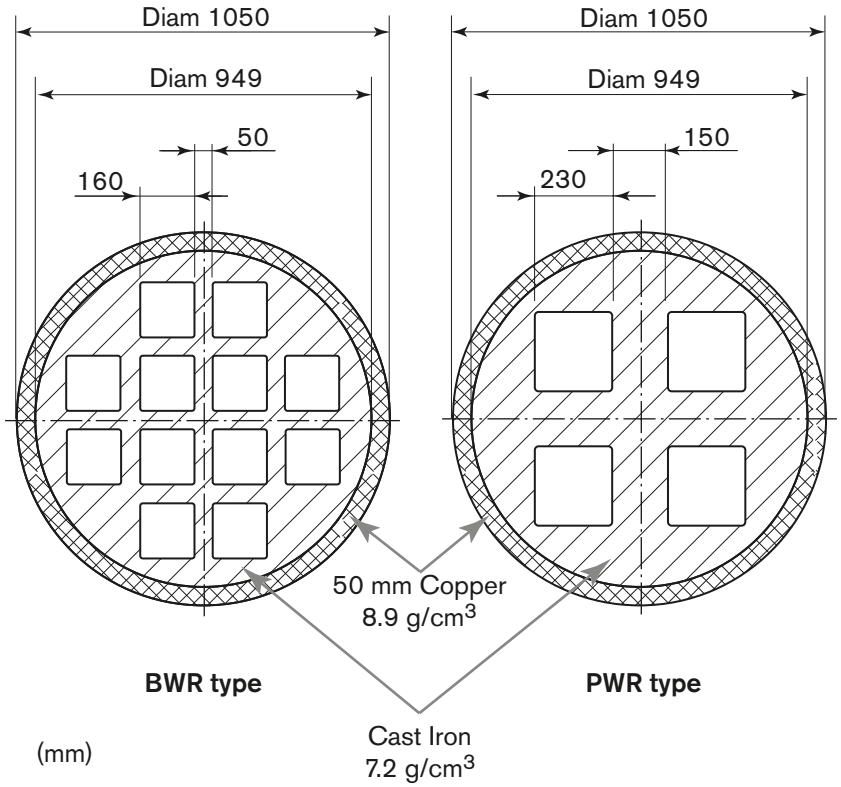

Figure 2-6. *The figure shows the schematic design of inserts for 12 BWR or 4 PWR assemblies for canisters with a 50 mm thick copper shell.*

Figure 2-7. *Welded cassette with 12 channels for BWR assemblies.*

Figure 2-8. *Casting of an insert.*

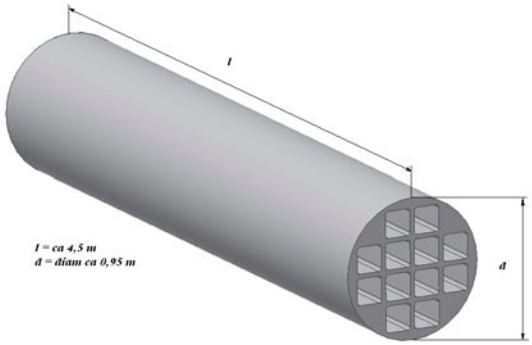

Figure 2-9. *General design of the cast iron insert.*

2.3.2 Possible defects in the cast iron insert

The discontinuities that have been identified in the cast iron insert are categorized as follows: shrinkage, porosity, sand and slag inclusions and crack-like defects. There are depicted in Figure 2-10 below:

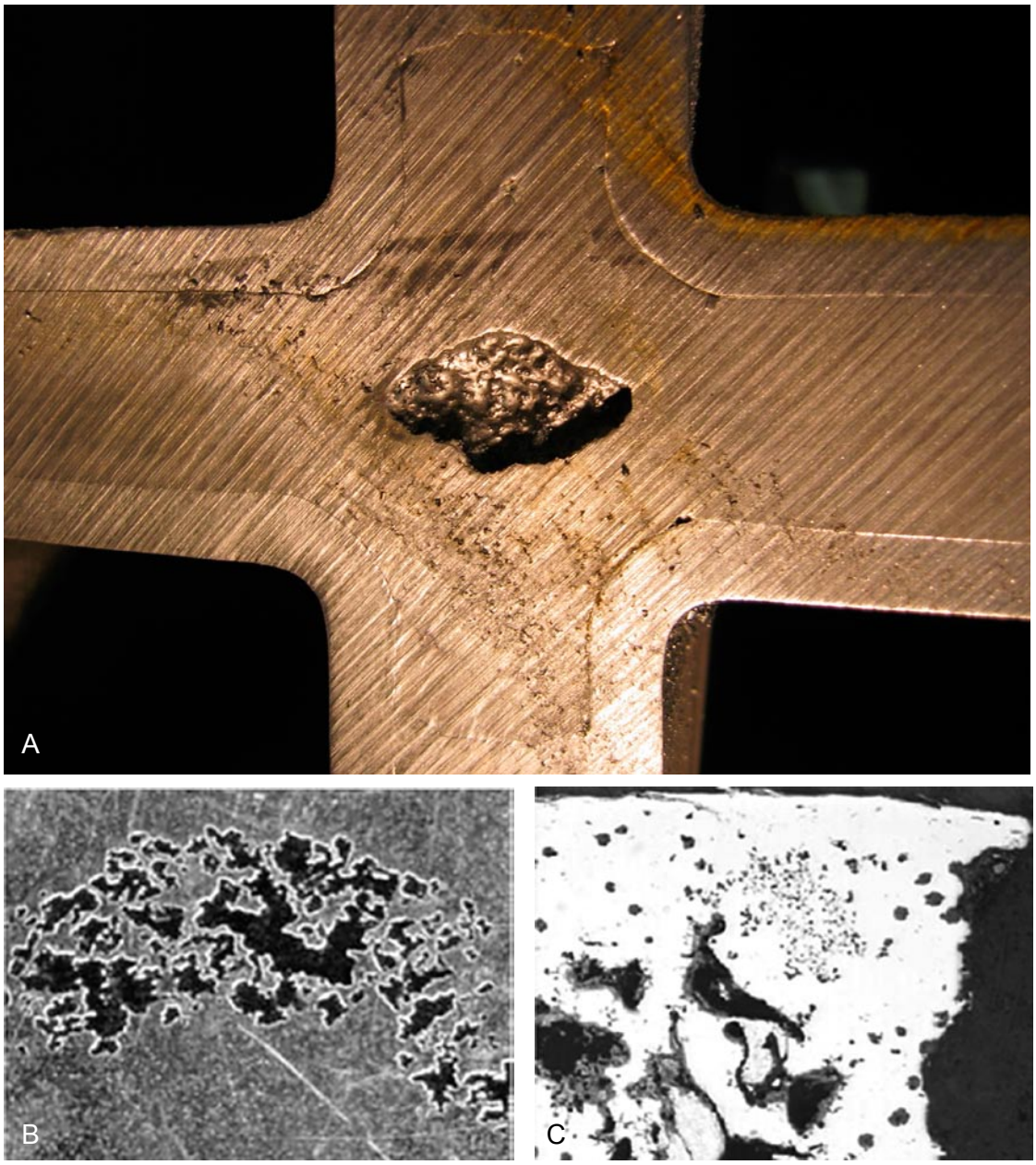

Figure 2-10. *Possible discontinuities in cast iron insert. (a) Shrinkage, (b) porosity and (c) slag inclusions.*

2.4 Welding of the lid/base and the tube

For sealing the canister, SKB developed a welding process called friction stir welding (FSW).

2.4.1 Welding process

FSW is a solid-state thermo-mechanical joining process, which is a combination of extruding and forging. A cylindrical shouldered tool with a profiled probe (pin) is rotated and slowly plunged into the material (Figure 2-11). For the thick sections, a pilot hole has to be drilled to make the plunge sequence possible without probe fracture. Frictional heat is generated between the wear-resistant tool shoulder and the material, causing the material to soften without reaching the melting point, and allowing the tool to traverse the joint line.

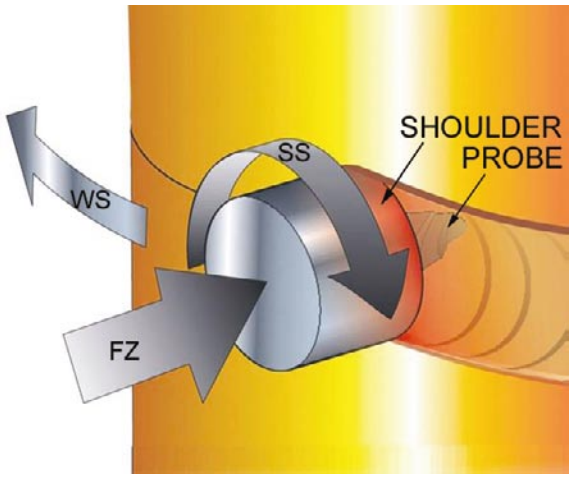

Figure 2-11. *Friction stir welding (SS=tool rotation speed, WS=welding speed, and FZ=axial force).*

One of the advantages of the FSW is the ease of process control due to the relatively few input parameters. The tool is rotated at a specified rotation rate and the tool is traversed along the joint line at a specified traverse rate. The tool is usually also tilted relative to the work piece so that the leading edge is above the surface. In order to create piece penetration the tool shoulder is controlled by applying a specified downward force or by specifying the position of the shoulder relative to the work piece. In addition to the input values, the tool temperature and the spindle motor torque are measured which provides an indication of the state of the process and the amount of frictional heat generated.

2.4.2 Possible defects in the weld

During the welding trials with FSW at the Canister Laboratory two types of defects have been found using relevant process parameter settings. These two types are named wormholes and joint line hooking (JLH), see Figure 2-12(a). The wormholes are located in the outer part of the weld and are more or less volumetric while the JLH are located in the weld root and is non-volumetric, see Figure 2-12(b) below.

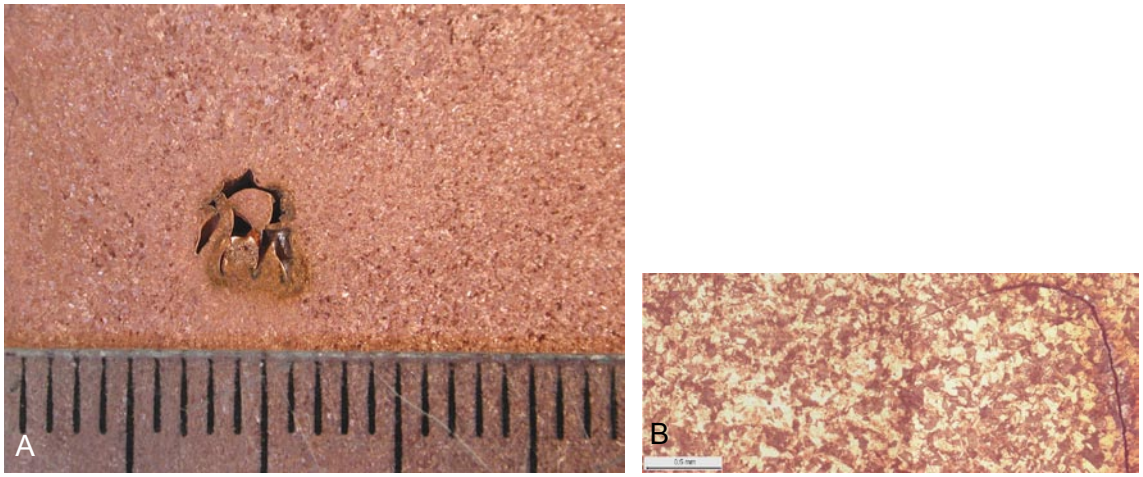

Figure 2-12. *Possible discontinuities in the welding part. (a) wormholes and (b) joint line hooking.*

3 Non-destructive testing by ultrasound

The main function of the canister, to ensure that its content does not come in contact with the environment, can be jeopardized if defects of certain properties are present in the material of the canister. To make sure that there are no such critical defects present, the components of the canister need to be tested. Non-destructive testing (NDT) is a type of testing which does not destroy the object and gives insight in the component structure. There are many methods of industrial NDT available such as ultrasonic testing, radiography, eddy current testing, visual testing and liquid penetrant.

SKB has in collaboration with Posiva developed ultrasonic techniques for NDT of the canister components. Ultrasonic inspection allows highly automated operation, only one surface of the tested object has to be accessible, the penetrating power and sensitivity enable the detection of even very small defects. The phased array ultrasonic system selected is an advanced technique for of ultrasonic testing. Together with the fully automated scanning process and data acquisition system it should adequately fulfil the inspection task.

The whole volume of canister parts has to be inspected for defects. Ultrasonic probes have to have access to different surfaces of parts to accomplish this task. Special manipulators are build to make manipulation of the large and heavy components possible.

3.1 General

To ensure repeatable inspections check-list based procedures have been established. The main task of the procedures is to determine the equipment (probes and fixtures), the reference objects, the scanning sequences and the ultrasonic settings to be used.

The probes and fixtures are positioned and adjusted at the reference object. The reference object is then scanned and the signals from the reference defects are analysed. After analysis, the object is scanned. The reference object is then scanned and evaluated once more, as a complementary verification. Finally, the data-files from the main object are analysed according to the established procedures.

3.2 NDT for copper tube

This section describes the NDT processes for the inspection of the copper tube.

3.2.1 NDT system for copper tube

For the inspection of the copper tube, SKB has a full-scale inspection system shown in Figure 3-1. The system consists of a manipulator for rotation of the tube as well as the reference object and a horizontal motion axis along the length of the component. The PLC-system for motion control, the phased array ultrasonic equipment and the fixture with the probes are placed at the horizontal axis. The phased array ultrasonic system is supplied by Technology Design Ltd. The main components are:

- Phased array system TD Focus-scan MKII.
- Linear array transducers of 80 elements with centre frequency of 5 MHz.
- Manipulator for rotation of the tube and positioning of transducers.
- Software (TD-Scan) for setting up the inspection and for the evaluation of results.

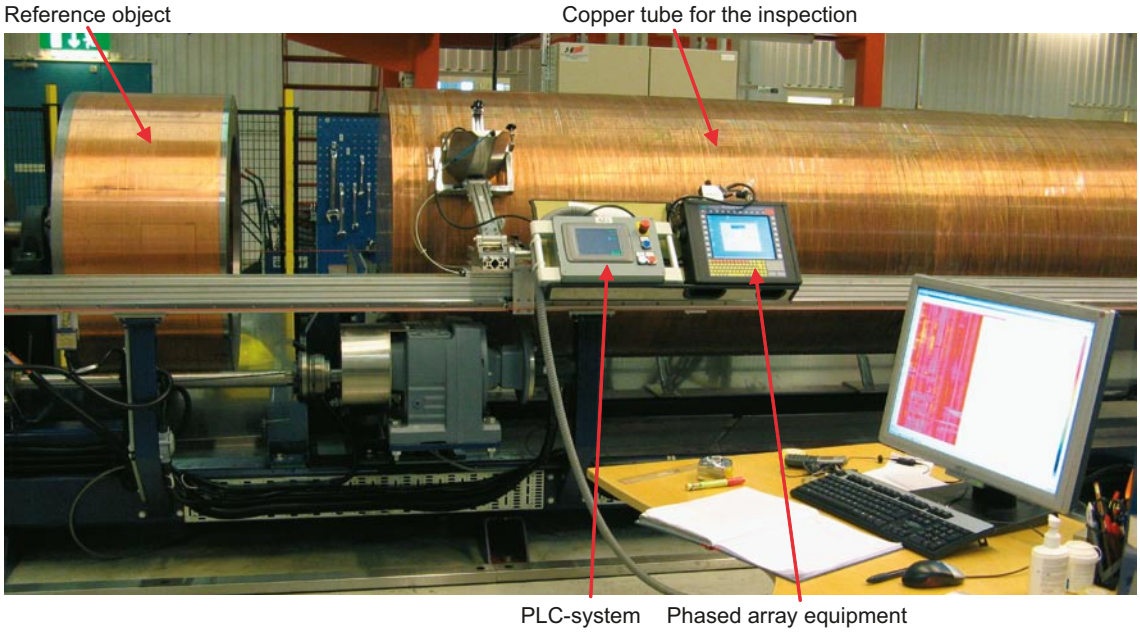

Figure 3-1. *System for the inspection of the copper tube.*

3.2.2 NDT processes for copper tube

The UT inspection is done with normal incidence waves with a 5 MHz linear array probe using immersion technique (see Figure 3-2) with a coupling solution of water mixed with a corrosion protection and a path of approximately 30 mm.

3.2.3 Test objects for copper tube

To estimate the reliability of NDT configurations, a numbers of test objects were manufactured with the same geometry (from the ultrasonic point of view) as the copper tube. A number of FBH's and SDH's were manufactured in the test objects.

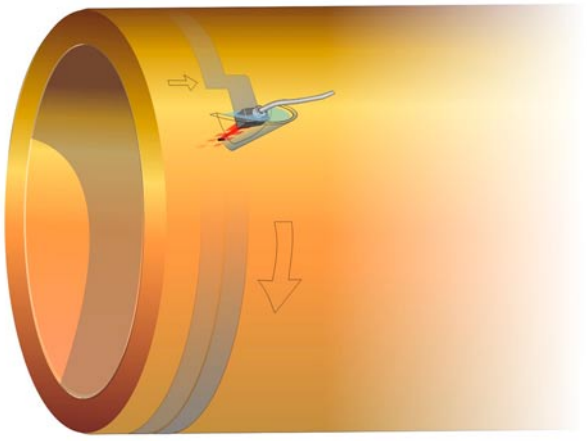

Figure 3-2. *Normal incidence inspection using immersion technique.*

3.3 NDT for copper lid/base

This section describes the NDT processes that are used for the inspection of the copper lids and bases.

3.3.1 NDT system for the copper lid/base

For inspection of the copper lid and base, SKB has a full-scale inspection system (Figure 3-4) that consists of a manipulator with an immersion tank for rotation of the lid and of a horizontal motion axis in radial direction of the component. The same PLC-system controls the manipulator and the same phased array ultrasonic equipment is used as for the other components. The phased array ultrasonic system is supplied by Technology Design Ltd. The main components are:

- Phased array system TD Focus-scan MKII, same as for the copper tube.
- Linear array transducers of 80 elements with centre frequency of 5 MHz.
- Manipulator for rotation of the lid and positioning of transducers.
- Software (TD-Scan) for setting up the inspection and evaluation of the results.

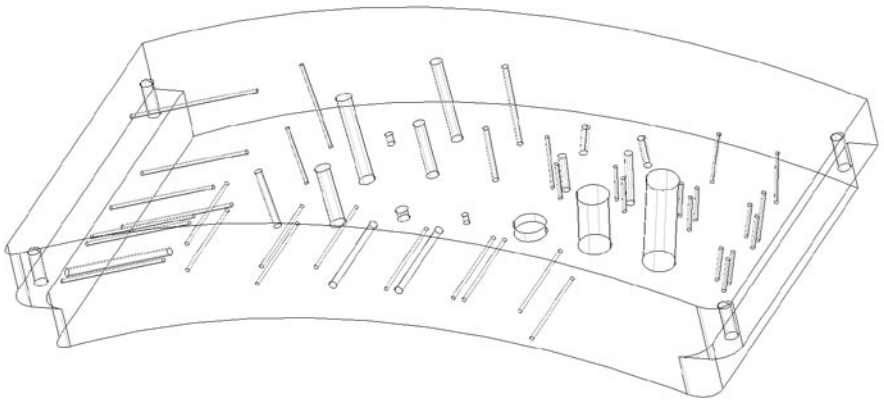

Figure 3-3. *One of the test objects for the NDT of the copper tube*.

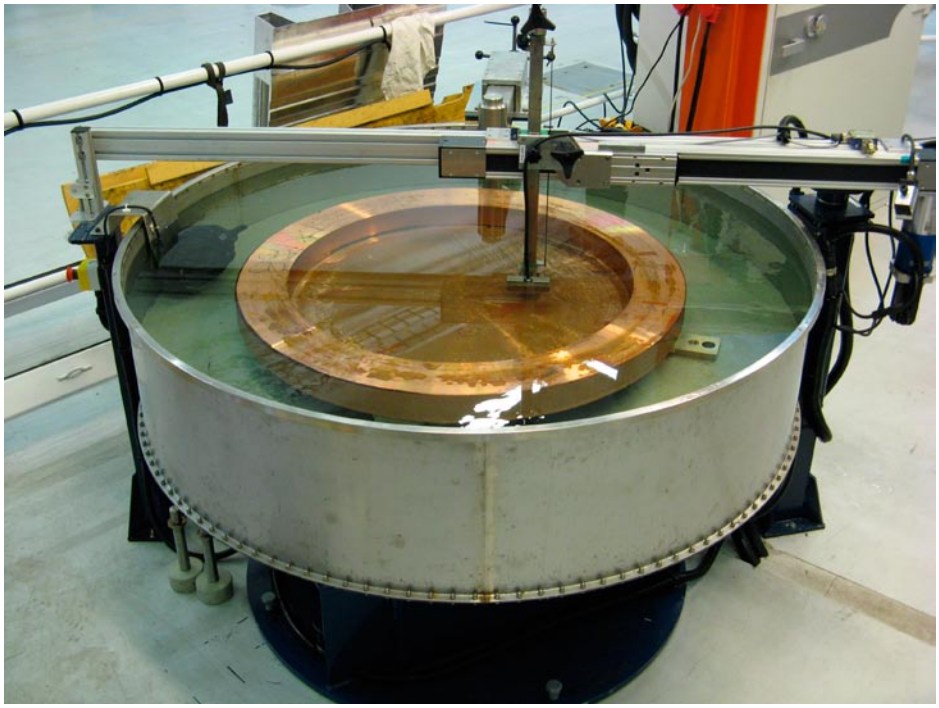

Figure 3-4. *System for inspection of copper lid/base.*

3.3.2 NDT processes for copper lid/base

From the NDT point of view, the lid can be divided into two parts; the inner thin area and the outer thicker area. The normal incidence inspection of the inner part of the lid is done with a 5 MHz linear array probe using immersion technique (see Figure 3-5(a)) with a coupling of water and a path of approximately 30 mm. The inspection of the outer part of the lid is done with the same array both in contact and immersion technique. Immersion technique is done from both the top and the envelope surface, with water path of 30 mm; see Figure 3-5(b) and (c).

3.3.3 Test objects for copper lid/base

To estimate the reliability of NDT configurations, a numbers of test objects were manufactured with the same geometry (from the ultrasonic point of view) as the copper lid/base. A number of FBH's and SDH's were manufactured in the test objects.

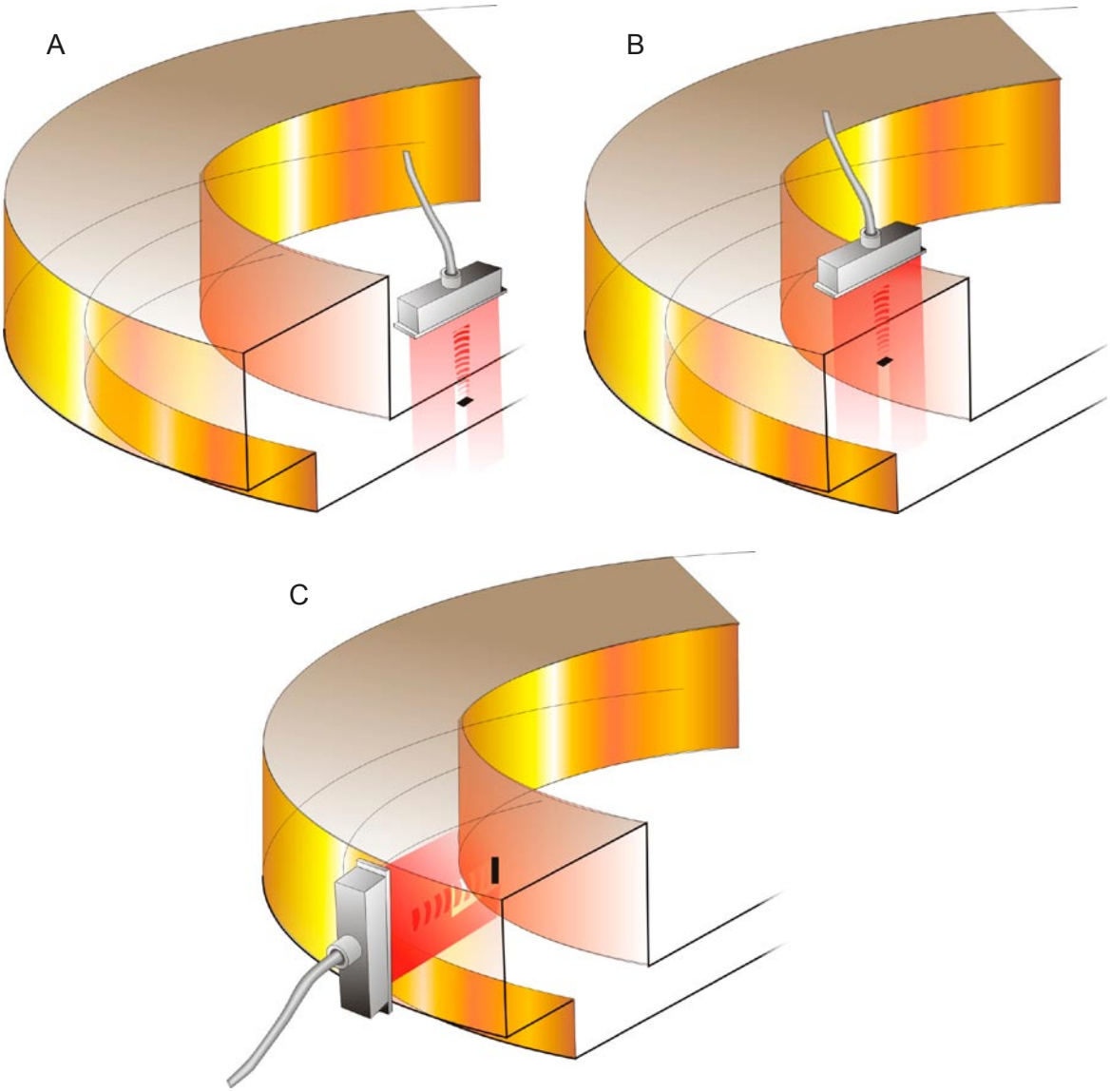

Figure 3-5. *Normal incidence inspection of the (a) centre part of the lid, (b) outer part of the lid from the top, and (c) outer part of the lid from the side.*

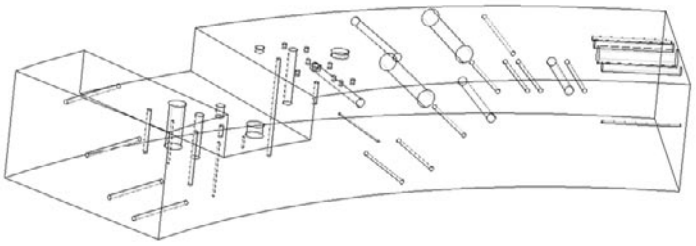

Figure 3-6. *Example of the test object for the NDT of the copper lid/base.*

3.4 NDT for cast iron insert

This section describes the NDT processes used for inspection of the cast iron insert.

3.4.1 NDT system for cast iron insert

For inspection of the cast iron insert, SKB uses the same full-scale inspection system as for the copper tube; see Figure 3-1. The main components are:

- Phased array system TD Focus-scan MKII, same as for the copper components.
- Linear array and curved surface transducers of 32 and 112 elements with centre frequencies of 1 and 2 MHz for the transmission technique and for the normal incidence inspection, respectively.
- TRL transducers with centre frequency of 2 MHz for the angle inspection.
- Manipulator for rotation of the insert and positioning of transducers.
- Software (TD-Scan) for setting up the inspection and evaluation of the results.

3.4.2 NDT processes for cast iron insert

For the non-destructive testing, the cast iron insert has been divided into three zones according to Figure 3-7. To cover the volume in these zones three different ultrasonic techniques are used.

- Normal incidence inspection.
- Angle inspection.
- Transmission technique.

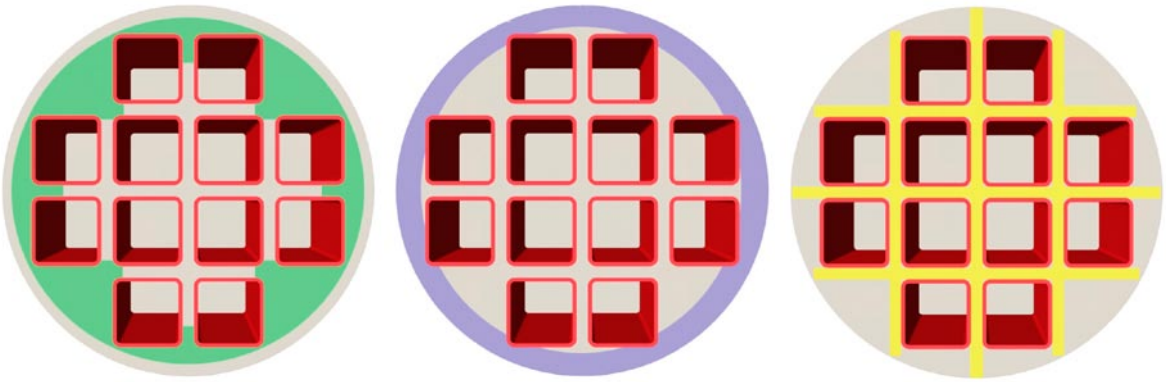

Figure 3-7. *Inspection zones of the cast iron insert. (a) Normal incidence inspection, (b) angle inspection, and (c) transmission technique.*

Normal incidence inspection

The normal incidence inspection is done with a 2 MHz linear array probe using immersion technique (see Figure 3-8) with a coupling solution of water mixed with a corrosion protection and a path of approximately 60 mm.

Angle inspection

The angle inspection (see Figure 3-9) is done with four 2 MHz TRL-probes (dual-crystal probe using longitudinal waves) with 70º incidence angle. The probes are directed with 90º separation and are placed in contact with the object using a squirting technique with the same coupling media as for the normal inspection.

Transmission inspection

The transmission inspection (see Figure 3-10) is done with two 1 MHz linear array probes that are placed on opposite sides of the insert. The insert is then scanned in axial direction in six steps, two in the centre and four off-centre, to cover all segments between the fuel channels. The probes are placed in contact with the object using a squirting technique with the same coupling media as for the normal inspection.

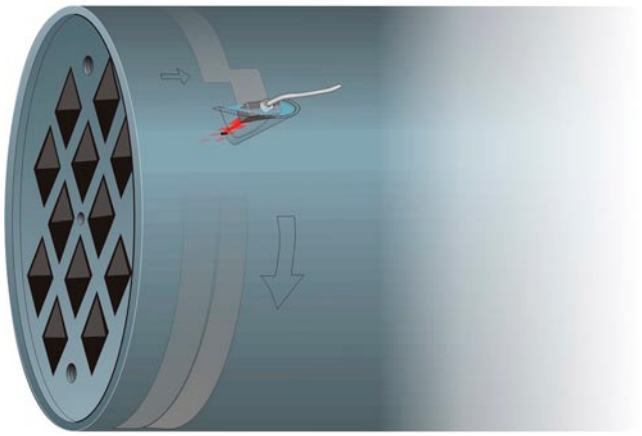

Figure 3-8. *Normal incidence inspection using immersion technique.*

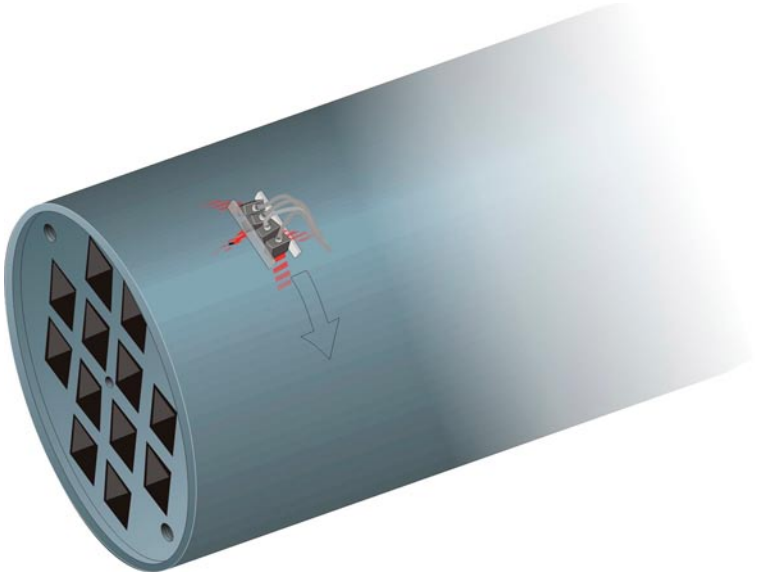

Figure 3-9. *Angle incidence inspection using contact technique.*

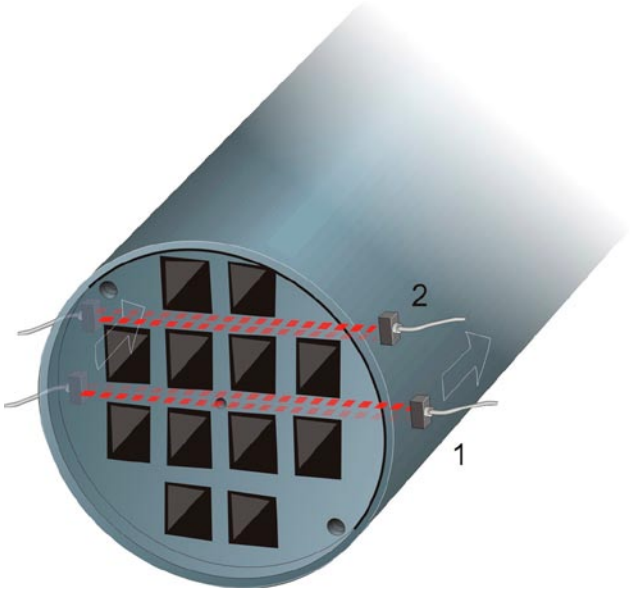

Figure 3-10. *Transmission inspection using contact technique; 1 – centre inspection, 2 – off-centre inspection.*

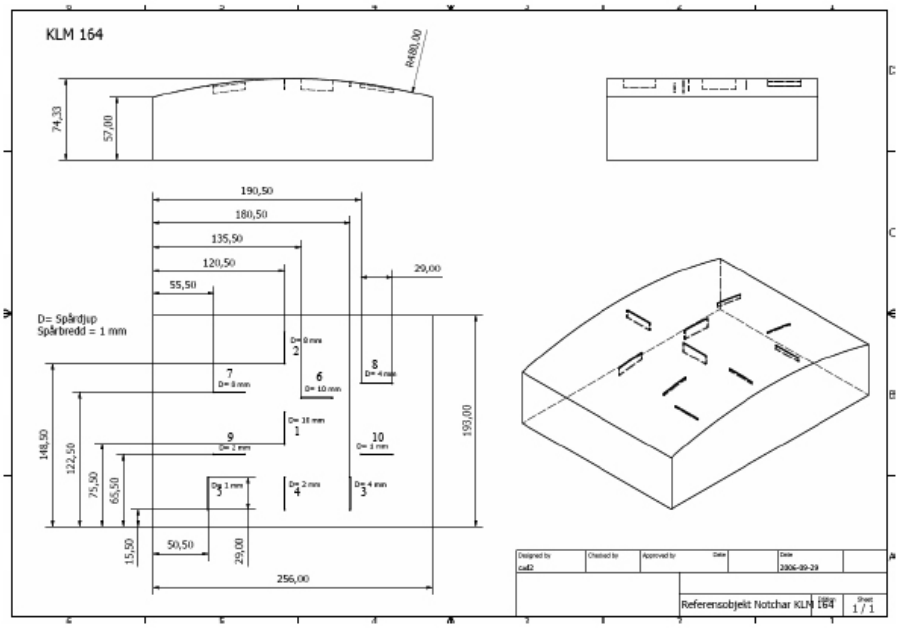

Figure 3-11. *One of the test objects for the NDT of the cast iron insert.*

3.4.3 Test objects for cast iron insert

To estimate the reliability of NDT configurations, a numbers of test objects were manufactured with the same geometry (from the ultrasonic point of view) as the cast iron insert. A number of FBH's, SDH's and notches were manufactured in the test objects.

3.5 NDT for friction stir welding (FSW)

This section describes the NDT processes used for the inspection of the friction stir welds.

3.5.1 NDT system for FSW

The phased array ultrasonic NDT system used for the FSW inspection is supplied by Technology Design Ltd., see Figure 3-12. The main components of the system are:

- Phased array system TD Focus-scan MKII, same as for the canister components.
- Linear array transducers of 80 elements with centre frequency of 5 MHz.
- Manipulator for rotation of the weld and positioning of the array transducers.
- Software (TD-Scan) for setting up the inspection and evaluation of the results.

3.5.2 NDT processes for the FSW

The main principle is that the canister rotates, while the array-transducer electronically sweeps the ultrasound in the radial direction of the canister. The transducer for the inspection of the FSW is a linear array with a centre frequency of 5 MHz. The inspection is made from the top of the canister lid (see Figure 3-13) with a thin water path which attains acoustical contact.

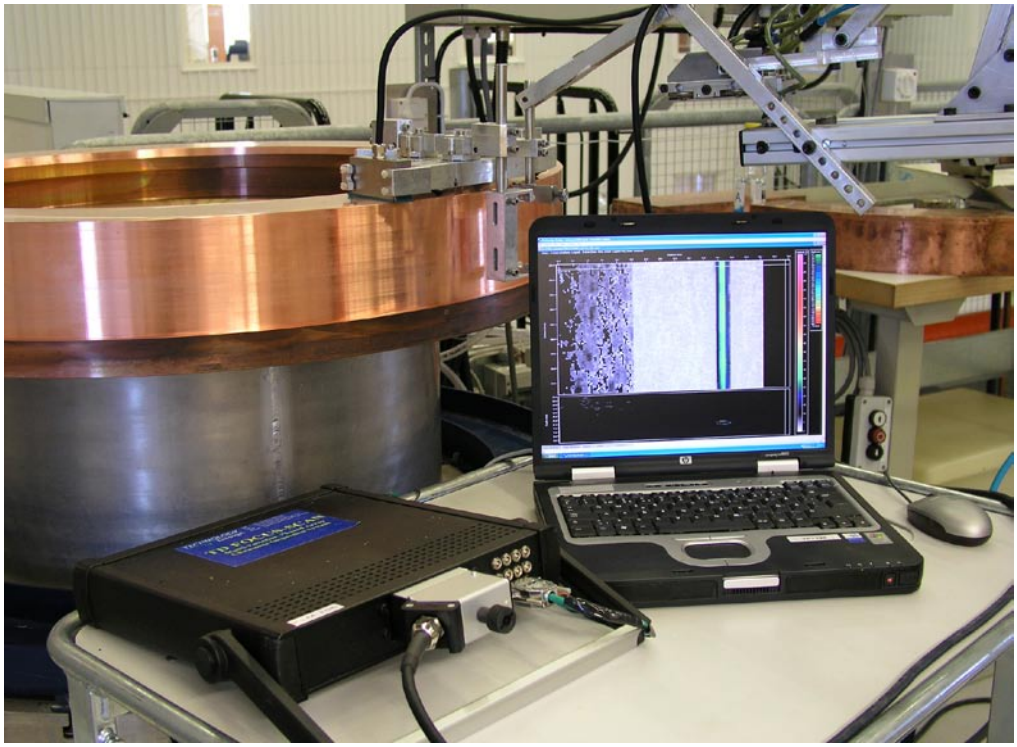

Figure 3-12. *Phased array system used for the inspection of the FSW at the Canister Laboratory.*

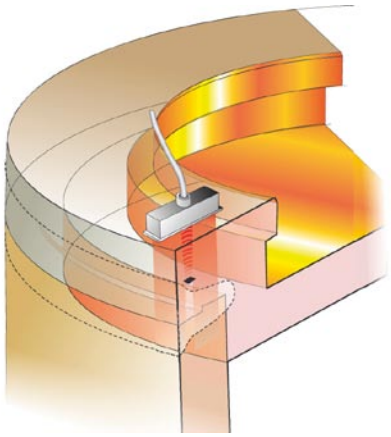

Figure 3-13. *Sketch of the phased array ultrasonic inspection of the FSW.*

4 Modelling

The ultrasonic simulation software employed for a part of the POD analysis in this project has been developed in BAM, division VIII.4 Acoustic and Electrical Methods. The principle of the modelling has been used in many applications for years /11–19/. The modelling was often used successfully for the probe design and the steering parameter optimisation. The programs for sound field and echo calculations use the point source synthesis (PSS) method taking into account the elastodynamic behaviour at the material boundaries. The method is briefly described in this chapter.

4.1 Principles of modelling

The simulation software calculates amplitudes of the sound pressure in time domain based on the point source synthesis method. The physical background of the method is Huygen's principle: each point of a wave front is the starting point of an elementary wave; the new wave front is obtained as the superposition of all elementary waves. Surfaces of the modelled transducers and reflectors are divided into a number of small patches, which are mathematically represented by point sources. The maximum size of the patches depends on the allowed phase shift between neighbouring patches (a small part of the wavelength, e.g. λ/7) in relation to the observation point. The elementary sound fields created by the point sources and described as the far fields of the point sources are superposed at the observation point considering the Snell's law at material interfaces, which can be flat or curved. The contributions of all point sources are additionally multiplied with the corresponding directivities. According to the principle, the complex sound pressure in frequency domain $\tilde{P}(\mathbf{r},\omega)$ at an observation point $\mathbf{r}$, in the case of an isotropic medium, can be computed by the following equation based on the Rayleigh integral.

$$\tilde{P}(\mathbf{r},\omega) = \sum_n \tilde{P}_0^n(\mathbf{r}_n,\omega)\frac{\exp\{-jk|\mathbf{r}-\mathbf{r}_n|\}}{|\mathbf{r}-\mathbf{r}_n|}\Gamma(\theta) \qquad (4\text{-}1)$$

where $\tilde{P}_0^n$ is a complex sound pressure created by the n-th point source assigned at a position $\mathbf{r}_n$. $k = \omega/v$ denotes a wave number in the material where v is the propagation velocity, and $\Gamma(\theta)$ is the directivity of the point source, both of them depend on the wave mode. The direction dependence of the directivities $\Gamma(\theta)$ is expressed as a function of θ, which is the propagation angle producing a contribution of the n-th point source in the direction ($\mathbf{r}$-$\mathbf{r}_n$). A detailed description of Eq. (4-1) and the determination of the directivities can be found in /20/. The summation in Eq. (4-1) of all those point sources results in the sound field and finally in an echo of a modelled flaw. Since the computation is in frequency domain, the inverse Fourier transform needs to be performed to $\tilde{P}(\mathbf{r},\omega)$ in order to obtain time domain responses of the sound pressure.

$$p(\mathbf{r},t) = F^{-1}\left[\tilde{P}(\mathbf{r},\omega)\right] \qquad (4\text{-}2)$$

Note that the sound field created by a point source $\tilde{P}_0^n$ in Eq. (4-1) is a far field solution. It is for a point source that is much smaller than the modelled transducer and reflectors, and it is sufficiently short distance for the near field of the modelled objects. Thus the method can also calculate the near field of the objects as shown below.

4.2 Simulation software

The simulation program is developed for one or two dimensional phased array probes and for a contact or immersion technique on plane or cylindrical surfaces. The result is the propagation of an acoustic pulse in time and space of the longitudinal and/or the transversal waves taking into account the geometry, the time delay distribution (focal law), the sound velocities, mode conversion factors, and attenuations in the wedge and the modelled material. The method calculates diffraction phenomena correctly, especially for the side and the grating lobes considering the geometry of the single element and the whole probe. Therefore the calculation can also be applied to short distances from the probe in the near field. The dynamic focusing technique applied in the phased array ultrasonic equipment used by SKB, has been implemented specially for this project. In the program, surface waves and multiple scattering between reflectors and between reflector and back wall are not calculated. The transmitting and the receiving probe can be separately modelled, e.g. to simulate a transmitter-receiver (TR) system or as a physical phased array probe with different focal laws, especially transmitting with a fixed focus and receiving with a dynamic focus. It enables to model various configurations used by SKB.

Figure 4-1 and Figure 4-2 show example results of the sound field calculation and Figure 4-3 and Figure 4-4 show the screen shots of the simulation software for the sound field and the echo calculations, respectively.

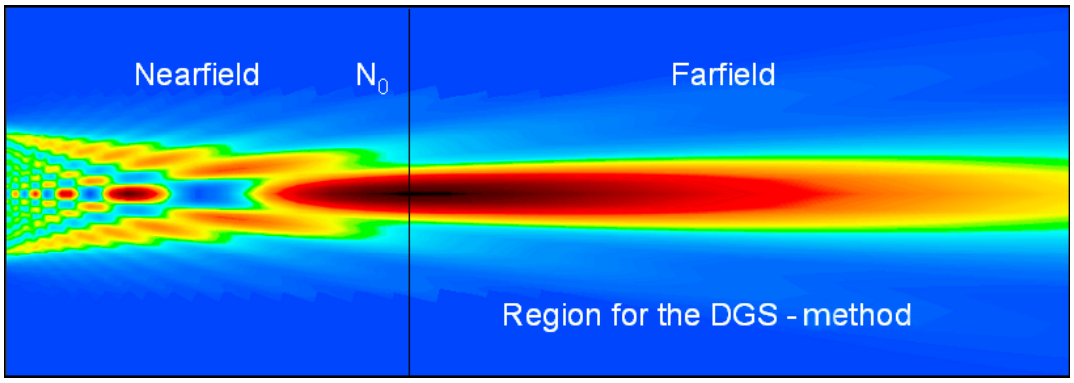

Figure 4-1. *Sound field calculated by the simulation program for a circular transducer with D/λ = 12.*

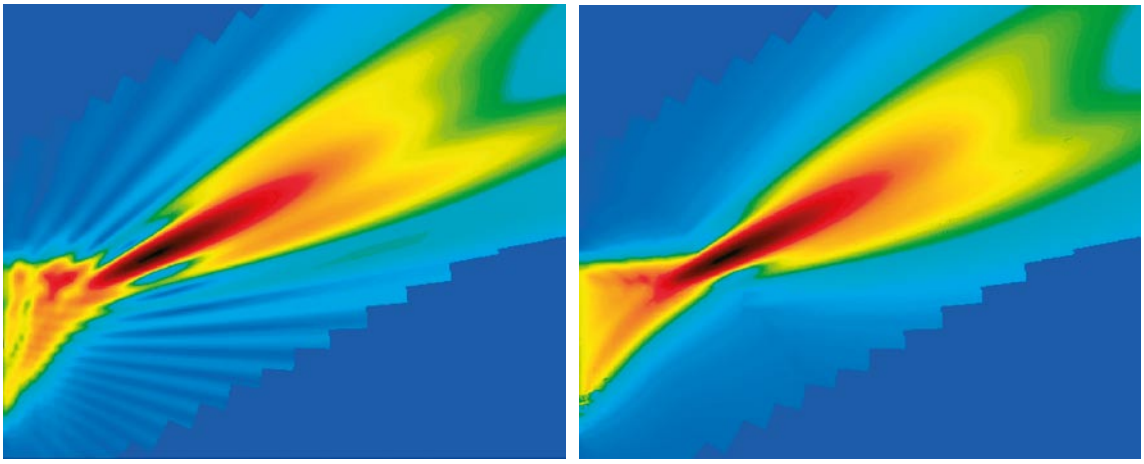

(a) **(b)**

Figure 4-2. *Sound field calculated by the simulation software for a focused and inclined phased array probe with 24 elements with D/λ = 10. (a) Continuous wave and (b) pulse with 30% bandwidth.*

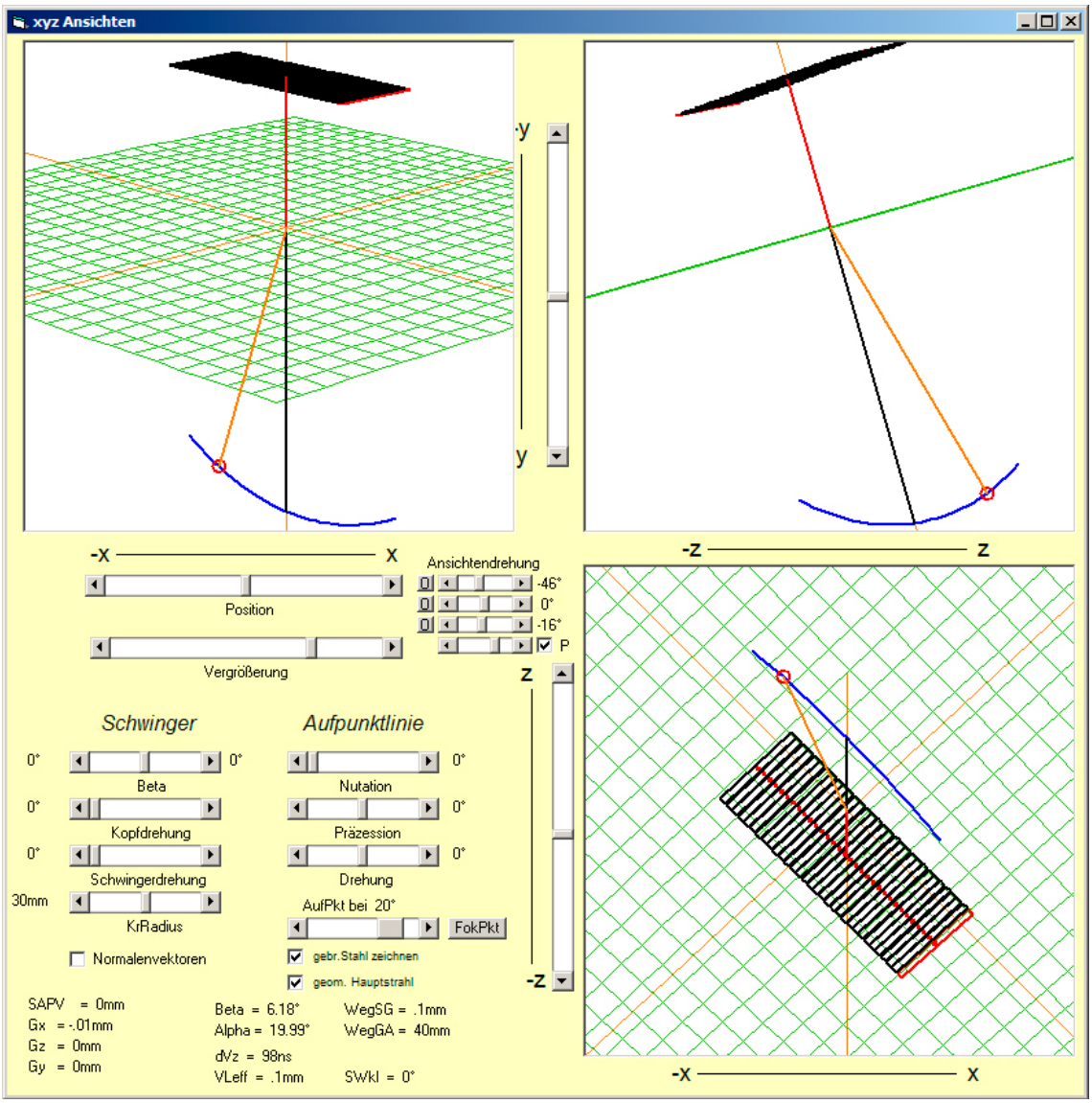

Figure 4-3. *Sketch of a modelled linear phased array probe; screenshot from the sound field calculation software.*

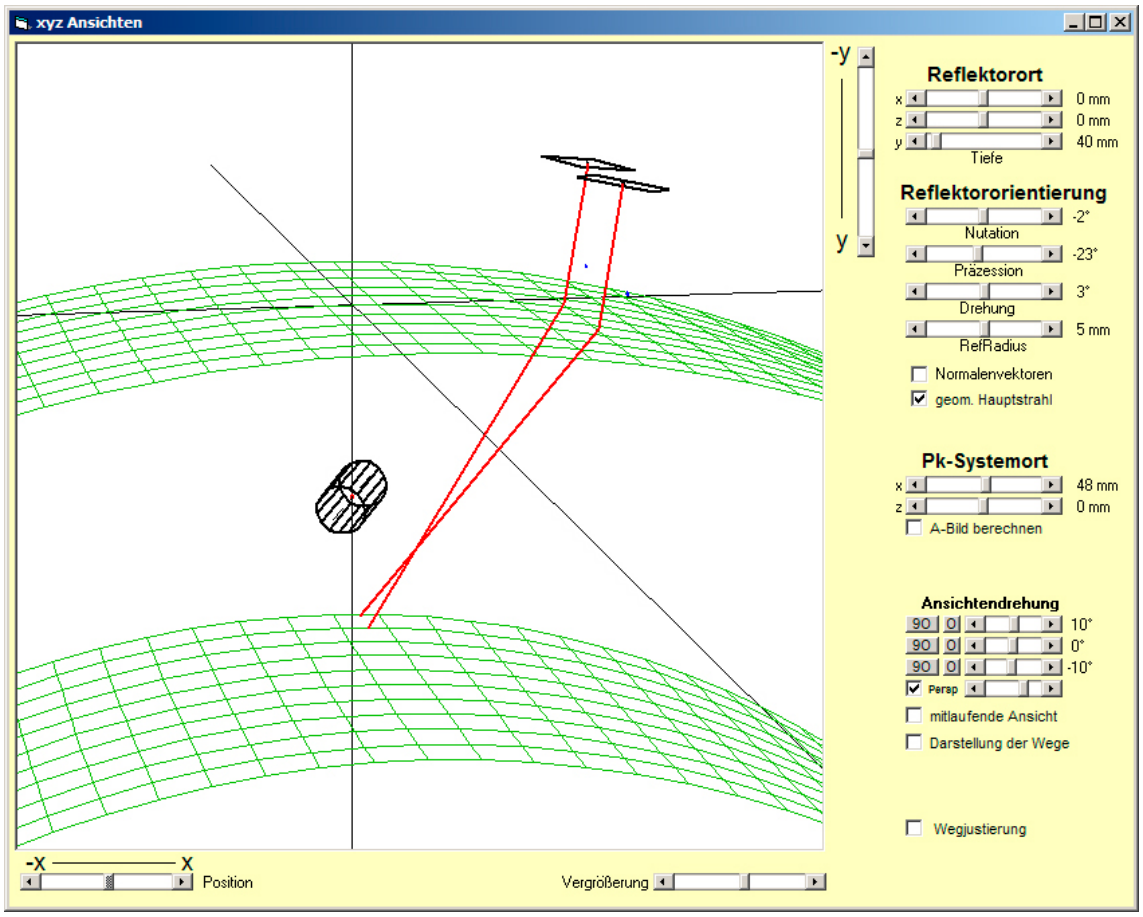

Figure 4-4. *Sketch of a modelled TR system and a SDH-like cylinder with the immersion technique; screenshot from the echo calculation software.*

5 Reliability analysis

In the conventional $\hat{a}$ versus a analysis, it is common to take the flaw size as a and the echo height from the flaw as $\hat{a}$. Applying this principle to phased array ultrasonic system results in highly scattered plots in the $\hat{a}$ versus a diagram. The reason of the scatter is that even if the flaw size may be the most dominant factor of the response, influences of the other factors are large and they can not be ignored. To achieve better estimation of the reliability of the ultrasonic NDT system, it is necessary to modify the conventional method to include the influence of these influencing factors in the model. Two approaches of the modification of the conventional method are developed within this project.

The first approach intends to include influences of several parameters on the POD, contrary to the only one parameter in the conventional method. For this purpose, a new definition of a is introduced, called the *multi-parameter a*. Additionally, a method that combines POD's given by multiple configuration measurements for the same test body is developed.

The second approach is modification of the definition of $\hat{a}$. The new definition includes more information on reflectors; not only the highest amplitudes is taken as the $\hat{a}$, as in the conventional method.

The first approach is called the *POD I* analysis and the second one the *POD II* analysis.

The conventional way to calculate the POD, described in details in /6/, is briefly presented in section 5-1. Modifications and developments are described in section 5-2 for the POD I analysis and in section 5-3 for the POD II analysis.

5.1 Conventional POD analysis

The principal of the POD analysis from signal response data, called $\hat{a}$ versus a evaluation is described in this section.

5.1.1 $\hat{a}$ versus a analysis

In a qualitative NDT system, a defect size (or depth) a is causing a signal amplitude (echo height) $\hat{a}$. If the signal exceeds a certain decision threshold $\hat{a}_{dec}$, the system gives a positive indication. As the NDT system is influenced by uncontrolled factors, defects having the same size cause signals of different amplitudes. The amplitude of the signal $\hat{a}$ to the size a is considered as a random value and is associated with a probability density $g_a(\hat{a})$. The relation between $\hat{a}$ and a can be expressed as:

$$\hat{a} = \mu(a) + \delta \qquad (5\text{-}1)$$

where $\mu(a)$ is the mean of $g_a(\hat{a})$ and δ is a random error term accounting for the differences between $\hat{a}$ and $\mu(a)$. The distributional properties of δ determine the probability density $g_a(\hat{a})$ about $\mu(a)$.

In practice, it is often assumed that δ is normally distributed with zero mean and a constant variance (independent of a). $g_a(\hat{a})$ is then the normal probability density function with mean $\mu(a) = 0$ and variance equal to that of δ.

The probability of detection (POD) function as a function of a can be obtained from the relation between $\hat{a}$ and a.

$$\mathrm{POD}(a) = \int_{\hat{a}_{dec}}^{\infty} g_a(\hat{a})\, d\hat{a} \tag{5-2}$$

This calculation is illustrated in Figure 5-1, in which the shaded area under the density functions represents the probability of detection.

5.1.2 Calculation of the POD

The parameters of the POD(a) function are calculated from parameters of the $\hat{a}$ versus a relation. The theory can also handle censored data, i.e. data below the recording threshold and above the saturation level, however this procedure is not described here because the data available from the NDT system of SKB does not contain any censored data.

A linear relation between $\ln(\hat{a})$ and $\ln(a)$ with normally distributed deviations has proved satisfactory. This model is expressed by

$$\ln(\hat{a}) = \beta_0 + \beta_1 \ln(a) + \delta \tag{5-3}$$

where δ is normally distributed with zero mean and constant standard deviation σ_δ. With the model, the POD function is calculated as

$$\begin{aligned} \mathrm{POD}(a) &= \mathrm{Probability}\left[\hat{a} > \hat{a}_{dec}\right] \\ \mathrm{POD}(a) &= \mathrm{Probability}\left[\ln(\hat{a}) > \ln(\hat{a}_{dec})\right] \\ \mathrm{POD}(a) &= 1 - \Phi\left[\frac{\ln(\hat{a}_{dec}) - \beta_0 + \beta_1 \ln(a)}{\sigma_\delta}\right] \end{aligned} \tag{5-4}$$

where Φ is the standard cumulative normal distribution function. Using the symmetry properties of Φ, Eq. (5-4) can be reduced to

$$\mathrm{POD}(a) = \Phi\left\{\frac{\ln(a) - \left[\ln(\hat{a}_{dec}) - \beta_0\right]/\beta_1}{\sigma_\delta/\beta_1}\right\} \tag{5-5}$$

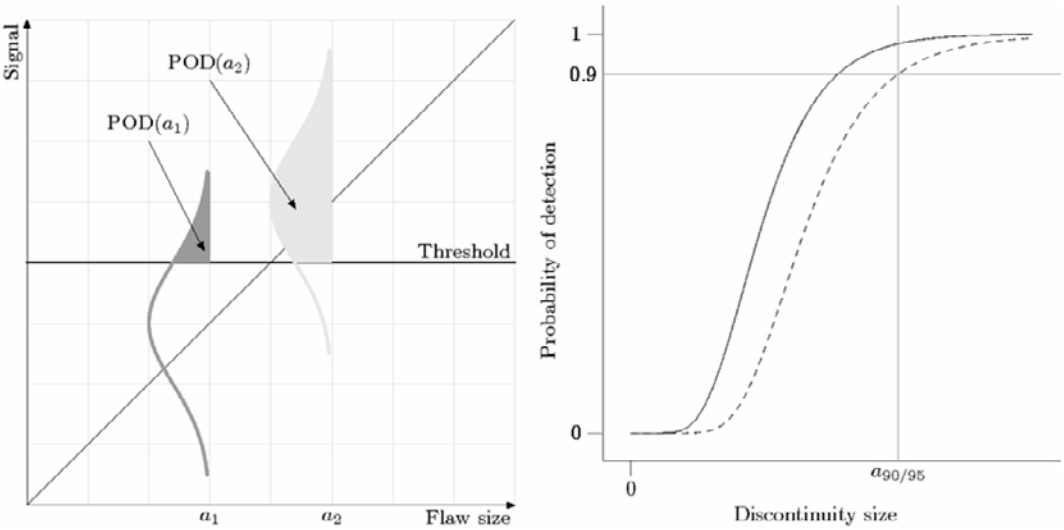

Figure 5-1. *(a) Schematic illustration of the POD calculation from the â versus a relation /4/ and (b) the POD curve with the lower 95% confidence bound.*

Eq. (5-5) is a cumulative log normal distribution function with mean and standard deviation of log crack size given by

$$\mu = \frac{\ln(\hat{a}_{dec}) - \beta_0}{\beta_1} \tag{5-6}$$

$$\sigma = \frac{\sigma_\delta}{\beta_1} \tag{5-7}$$

The parameters β_0, β_1 and σ_δ need to be estimated to calculate the POD function, and the estimations can be given by the maximum likelihood method.

5.1.3 95% Confidence bounds

The lower one-sided 95% confidence bound of the POD(a) is given by

$$\mathrm{POD}_{95}(a) = \Phi(\hat{z} - h) \tag{5-8}$$

where

$$\hat{z} = \frac{\ln(a) - \hat{\mu}}{\hat{\sigma}} \tag{5-9}$$

and h reflects the sample size and the scatter of the source data. It is defined as

$$h = \sqrt{\frac{\gamma}{nk_0}\left[1 + \frac{(k_0\hat{z} + k_1)^2}{(k_0k_2 - k_1^2)}\right]} \tag{5-10}$$

where γ can be obtained from Table 5-1 for the number of samples in the experiment. The calculation of the values is thoroughly explained in /21/ and /22/. The variables k_0, k_1 and k_2 are the components of the information matrix $\mathbf{I}$ for the assumed POD(a) model with parameters $\boldsymbol{\theta} = (\mu, \sigma)^T$ as

$$\mathbf{I}(\mu,\sigma) = \frac{n}{\sigma^2}\begin{bmatrix} k_0 & -k_1 \\ -k_1 & k_2 \end{bmatrix} \tag{5-11}$$

Table 5-1. Values of γ for 95% lower confidence bounds on the POD(a) function. (Source /6/).

Sample size	γ for 95% confidence level
20	5.243
25	5.222
30	5.208
40	5.191
50	5.180
60	5.173
80	5.165
100	5.159
∞	5.138

where n is number of defects in the experiment. The information matrix is defined as inverse of the variance-covariance matrix of $\hat{\mu}$ and $\hat{\sigma}$ given by

$$\mathbf{V} = \mathbf{I}^{-1} \tag{5-12}$$

and

$$\mathbf{V}(\mu,\sigma) = \frac{1}{\beta_1^2}\mathbf{T}\mathbf{V}(\hat{\beta}_0,\hat{\beta}_1,\hat{\sigma}_\delta)\mathbf{T}^T \tag{5-13}$$

where $\mathbf{V}(\hat{\beta}_0,\hat{\beta}_1,\hat{\sigma}_\delta)$ is the variance-covariance matrix of the maximum likelihood estimates of the $\ln(\hat{a})$ versus $\ln(a)$ analysis and $\mathbf{T}$ is the transform matrix defined by

$$\mathbf{T} = \begin{bmatrix} 1 & \mu & 0 \\ 0 & \sigma & -1 \end{bmatrix} \tag{5-14}$$

5.2 The POD I analysis

In the POD I analysis, as already mentioned, intention is to include influences of several parameters on the POD. For this purpose, a new definition of a called the *multi-parameter a* is introduced. In addition, a method that combines POD's given by multiple configurations measurements for the same test body is developed.

5.2.1 Multi-parameter *a*

The $\hat{a}$ vs. a method described in the previous section, where the signal response of the inspection system (eddy current) is correlated with only one characteristic of the flaw (flaw length), had to be modified for the case of complex interaction between the sound field of the ultrasonic phased array system and the flaw. The flaw that might occur in the material can be of any arbitrary shape. It is hard to predict the response of such flaw, so the analysis is based on the response of the flat-bottom holes (FBH). These are geometrically simple, artificial flaws whose response can be calculated by the computer simulation. They can also be manufactured in different sizes, depths and orientations so that the model calculation can be validated by the experiment.

The reflection amplitude A from the FBH can be expressed as a function of many influencing parameters:

$$A = f(x_1, x_2, ..., x_n) \tag{5-15}$$

The list of influencing parameters is long as shown in /23/; in our analysis we consider the influences of depth z, size (diameter) d and orientation (tilt angle) β of the FBH as the most dominant ones. By this selection of influencing parameters, Eq. (5-15) can then be simplified as:

$$A = f(z, d, \beta) \tag{5-16}$$

Although the amplitude is now expressed as a function of only three parameters, those parameters are also influenced by other parameters. For example, the amplitude change due to depth is also depending on sound field formed by the probes which is depending on frequency, probe configuration, wedge, focal laws, velocity of sound in material and so on.

To investigate these influences on the response of the FBH computer simulation is used, varying three selected parameters. The calculation of the sound field and the echo response of the FBH were simulated with the BAM simulation software, described in Chapter 4. The echo response is calculated from the simulation for various depths, diameters and orientations of the FBH and modelled amplitudes A_{model} are obtained for discrete z, d and β:

$$A_{model} = f(z, d, \beta) \tag{5-17}$$

as shown in Figure 5-2. To achieve a continuous expression of the function *f* and to be able to calculate the response for every value of the depth, diameter and orientation of the FBH, a function is fitted to the simulated echo response

$$A'_{model}(z,d,\beta) = P_1(z)e^{C_1 z^2} P_2(d)e^{C_2 d^2} P_3(\beta)e^{C_3 \beta^2} \quad (5\text{-}18)$$

where P_1, P_2, and P_3 are polynomials in z, d, and β, respectively, and C_1, C_2 and C_3 are coefficients of the exponential terms. Figure 5-3 shows the fitted surface of the modelled amplitudes for depth and diameter of the FBH.

Attenuation in the material is not calculated by the simulation. The amplitude change in z direction due to the attenuation can be written in form of an exponential function $e^{-\alpha z}$, where α is the attenuation coefficient. The α is estimated from the experimental data. The ultrasonic phased array system creates non-uniform sound field as depicted in Figure 5-4 and the energy of the sound waves attenuates as they propagate through the material. These influences are also included in the calculation.

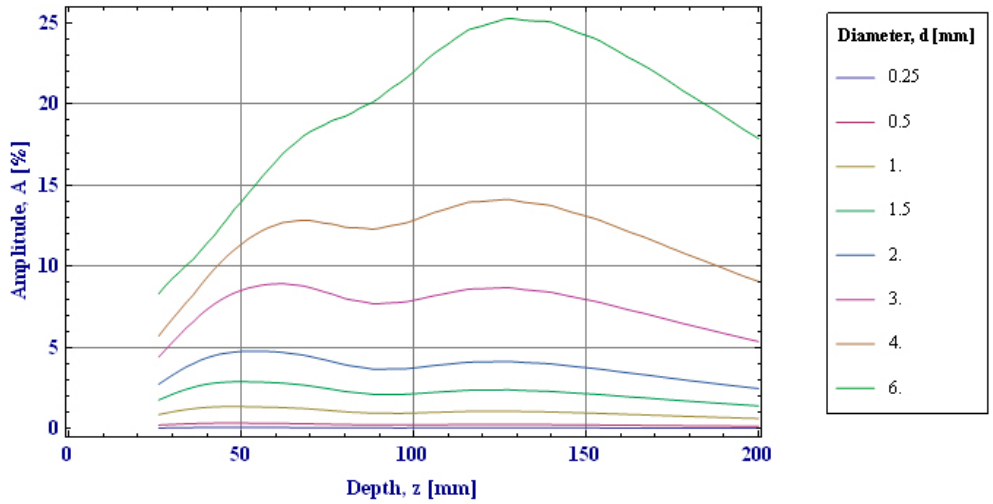

Figure 5-2. *Dependence of the amplitude for the FBH with angle of orientation of 0° with the depth, for different diameters of the FBH (simulation for the normal incidence, contact technique configuration, 32 elements, Tx focal depth = 200 mm, Rx focal depth = 45–200 mm; dynamic focusing).*

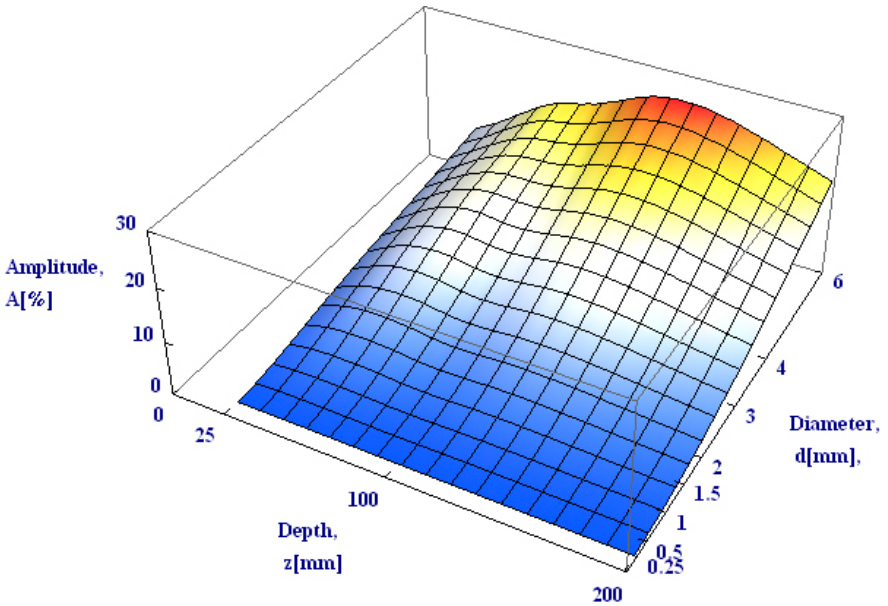

Figure 5-3. *Amplitude dependence of the FBH on the diameter and depth, with orientation β = 0° FBH (simulation for the normal incidence, contact technique configuration, 32 elements, Tx focal depth = 200 mm, Rx focal depth = 45–200 mm; dynamic focusing).*

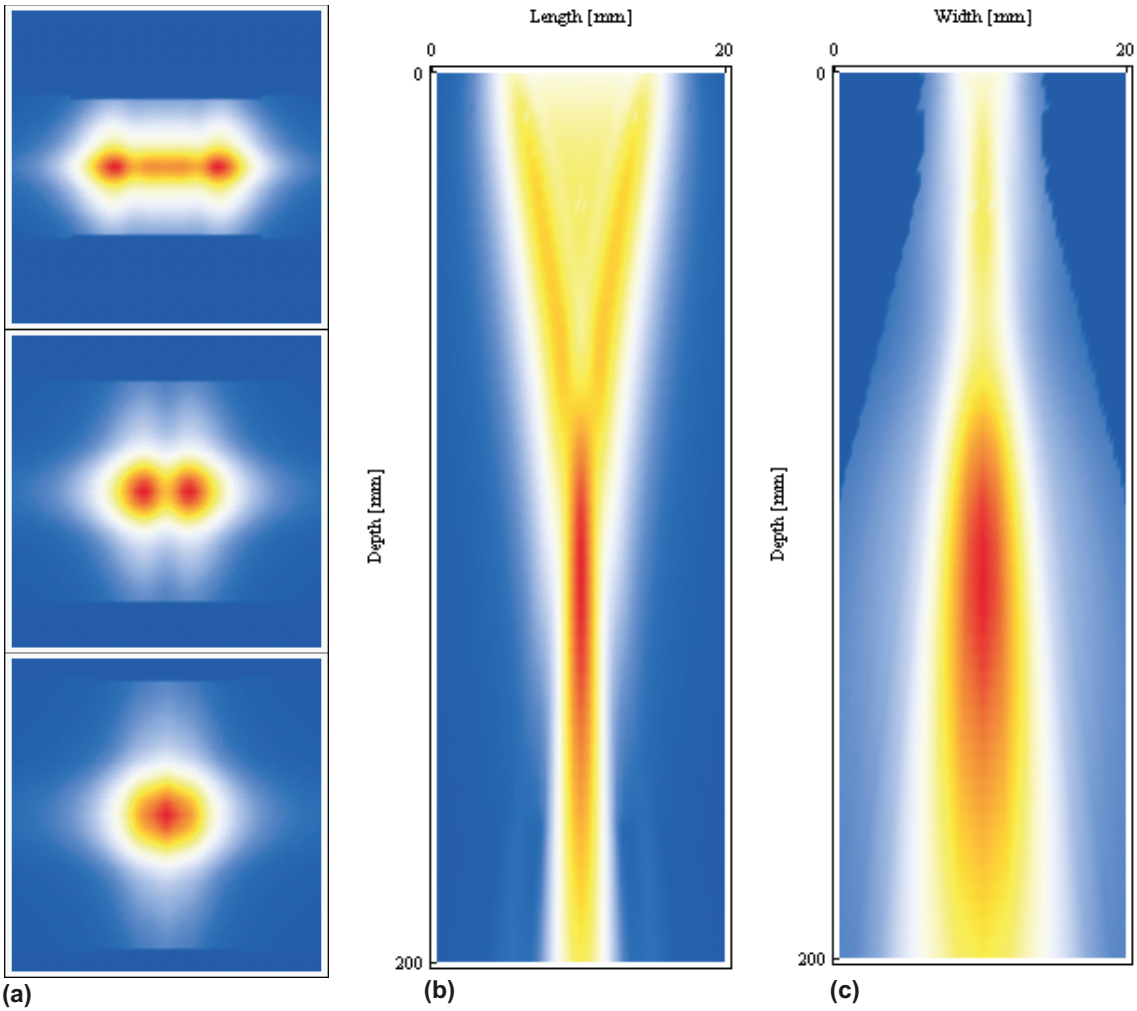

Figure 5-4. *Simulation of the sound field for the normal incidence, contact technique configuration; 32 elements, Tx focal depth = 200 mm, Rx focal depth = 45–200 mm – dynamic focusing; (a) Horizontal cross sections of the sound field at different depths, (b) vertical cross section in the plane of focusing and (c) in the perpendicular plane.*

Additionally, we need to scale ("calibrate") simulated response to the measured values of the response with a coefficient C_s

$$A''_{model}(z,d,\beta) = A'_{model}(z,d,\beta)e^{-\alpha z}C_S \tag{5-19}$$

As $\hat{a}$ value we use measured amplitude

$$\hat{a} := A_{meas} \tag{5-20}$$

As a value we use the estimated amplitude, calculated from the simulation:

$$a := A''_{model}(z,d,\beta) \tag{5-21}$$

As it can be seen in Eqs. (5-17)–(5-19) and (5-21), the definition of a in this analysis is a function of many parameters. Thus the a is called *multi-parameter a*.

The measured amplitude $\hat{a}$ is then plotted against the estimated a to create a diagram corresponding to the conventional $\hat{a}$ versus a diagram, as shown in Figure 5-5. Linear regression is performed and 95% confidence bands are calculated /6/. If the model would completely describes the phenomena and the experimental measurement would be without errors, then the regression line would have a slope 1 and pass trough zero and points would lie exactly on the regression line. Since in reality this is not the case, the regression line deviates from the ideal one and the data are scattered around the regression line.

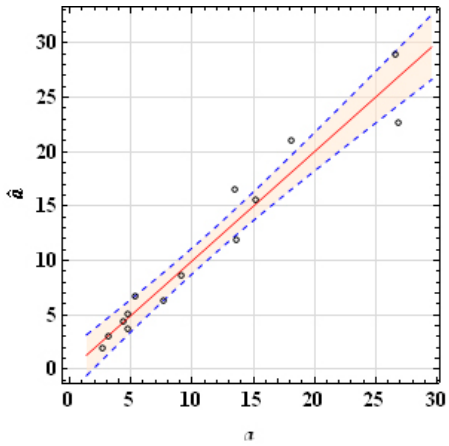

Figure 5-5. *Scatter plot of the measured and calculated amplitude, regression line and 95% confidence bands.*

Setting the threshold and assuming that the error is normally distributed, the POD can be calculated as shown in Figure 5-6. The threshold is set conservatively at the level 3 SNR. The POD curve is obtained as a function of multi-parameter *a* and it is not physically interpretable. By varying only one and fixing other two parameters in Eq. (5-21), the POD curve can be decomposed into curve for only one parameter. Figure 5-7 shows the POD curves plotted against diameter, depth and angle. In the figures, the POD increases with increasing diameter and decreases with increasing depth and orientation angle of the FBH's. This behaviour agrees with physical laws and our experience.

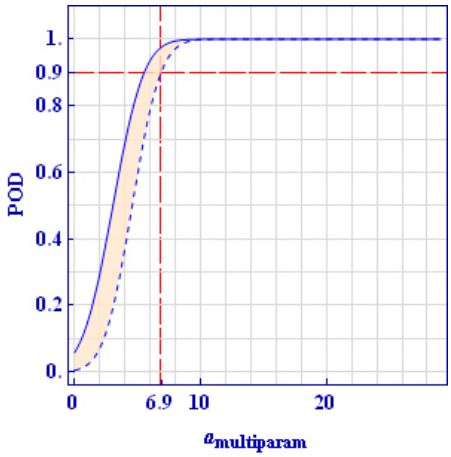

Figure 5-6. *The POD curve plotted against the multi-parameter a.*

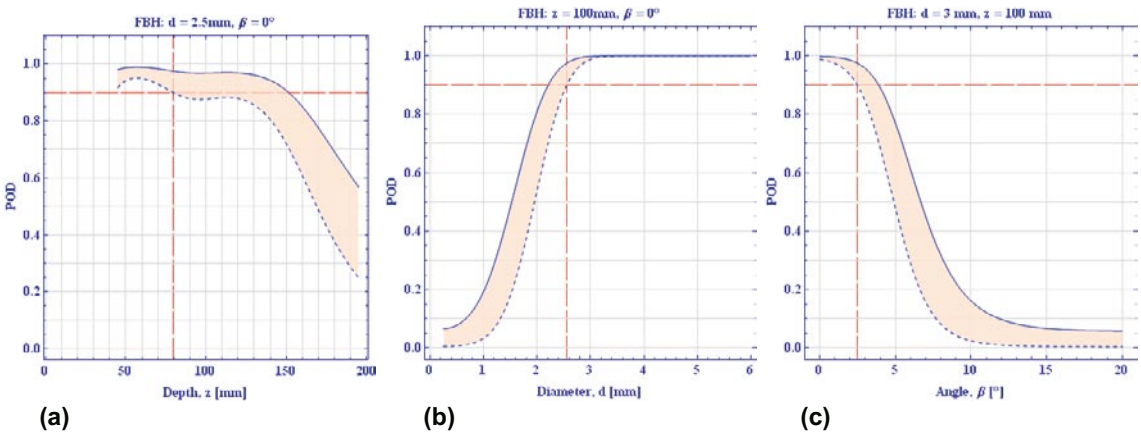

Figure 5-7. *The POD curves with the lower 95% confidence bands with indicated a90/95 point, plotted against (a) depth, (b) diameter, and (c) angle.*

Furthermore, the POD curve with respect to the depth is not simple but it reflects intensity variation of the sound field created by the phased array probe as one can see in Figure 5-4. Therefore the POD analysis with new definition of *a* allows more detailed observation of the POD curve variation depending on the physical parameters.

As a measure of acceptance of the NDT configuration the lower 95% confidence band is used. In Figure 5-8, for clarity, only lower confidence bands are shown. From the diagram it can be seen that the UT configuration fulfils its task if the critical FBH has diameter of 4 mm or higher, across the whole range of depths. If the critical FBH has a diameter of 3 mm, additional inspection is needed for the depths between 160 and 200 mm.

5.2.2 The POD of the flaw in the volume

The diagrams presented in the previous section show the POD of the individual UT configurations of defects in the material. When the material is inspected with only one UT configuration, the POD given by the configuration is at the same time the total probability to detect a defect.

$$POD_{total} = POD_1 \tag{5-22}$$

When the volume of material is inspected with more than one UT configuration, individual POD's are not identical to the total probability; they only give probabilities of individual configurations to detect a defect.

$$POD_{total} \neq POD_1 \neq POD_2 \neq \ldots \neq POD_n \tag{5-23}$$

The individual and total probabilities can be rather different because the same defect will not appear the same to the different configurations. Because of the orientation, the same defect can reflect significant amount of sound waves in one direction, and a very small amount in the perpendicular direction. In Figure 5-10, the probe S_1 will receive much more reflected energy from the defect than the probe S_5. The UT configuration that would receive larger amount of reflected sound waves would also give a higher POD, and the configuration receiving smaller amount of reflected waves would give lower POD. The actual probability that the defect will be detected is determined by the total POD of *n* UT configurations, not by the POD of the individual configuration.

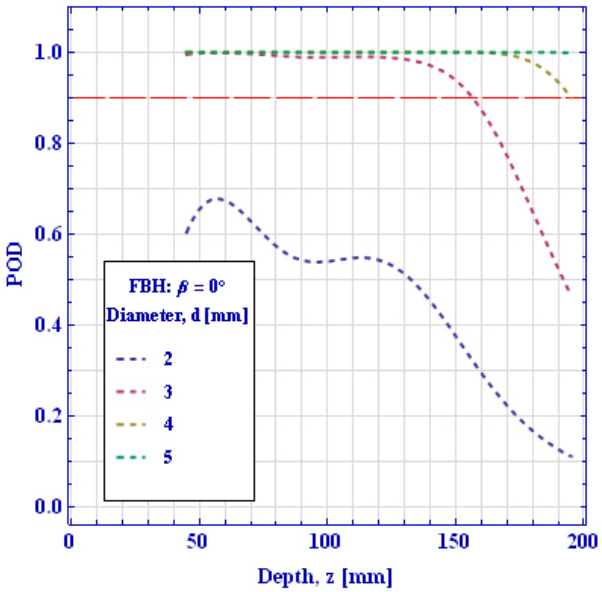

Figure 5-8. *The lower 95% confidence bands for the FBH vs. depth z, for fixed value of the angle β and different diameters d.*

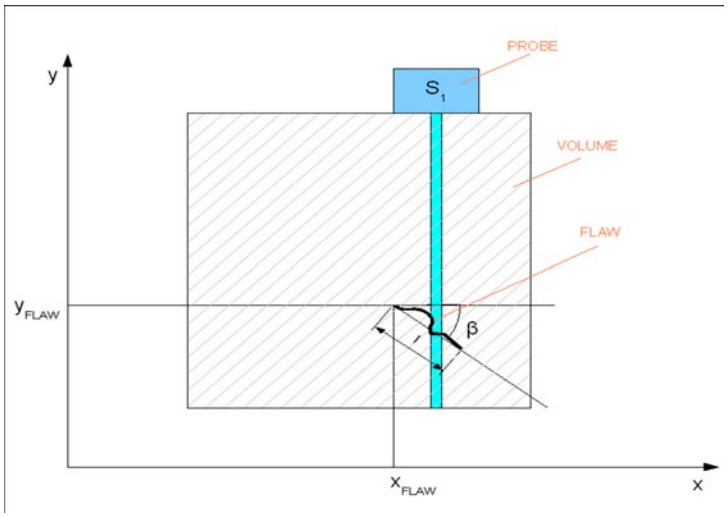

Figure 5-9. *Inspection of the material with one UT configuration.*

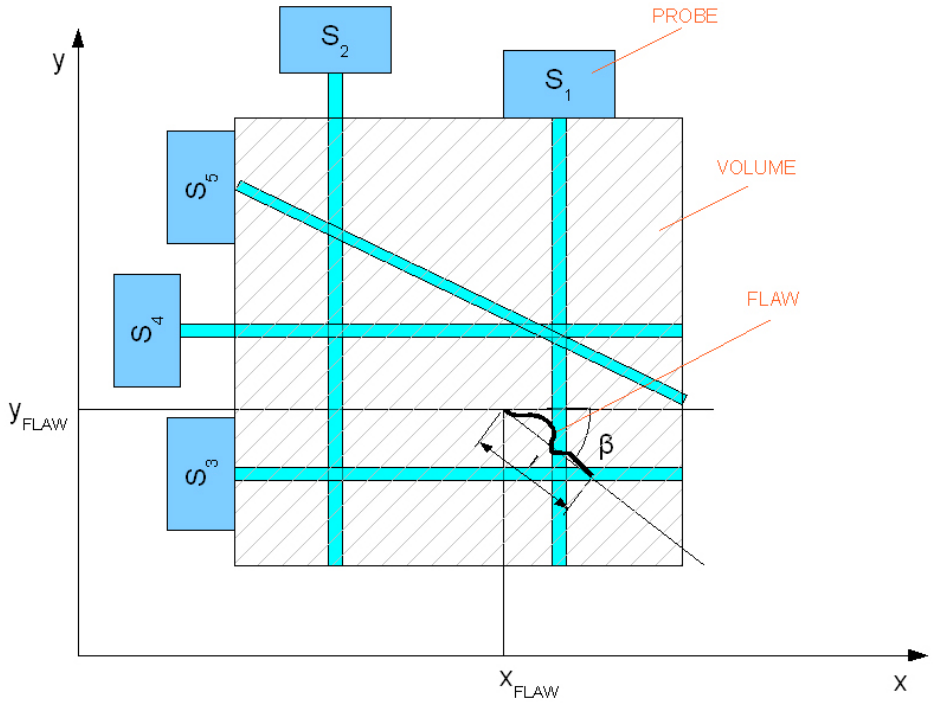

Figure 5-10. *Inspection of the material with several UT configurations from different sides.*

If the independency of configurations is assumed, the probability that the defect will be missed when the volume is inspected with *n* configurations can be expressed as a product of individual probabilities to miss the defect:

$$(1 - POD_{TOTAL}) = \prod_{i=1}^{n} (1 - POD_i) \tag{5-24}$$

Therefore, the total POD obtained by *n* configurations is given by

$$POD_{TOTAL} = 1 - \prod_{i=1}^{n} (1 - POD_i) \tag{5-25}$$

Knowing the POD of the individual UT configurations, overall POD in the volume of material can be calculated – the volume POD. This way of displaying the POD gives us direct and easily understandable view about the design of the inspection system. The regions in the volume which are not sufficiently inspected and also regions which are inspected more than necessary to reach sufficient level of reliability can be clearly identified. This information can be used to optimise the design of the system. This way, the volume POD is used not only as the final judgment of the reliability of the inspection system, but also as an optimisation tool.

It can be assumed that different regions of the inspected part will have different acceptance criteria based on the size and orientation of the defect. If instead of the POD, the lower 95% confidence band is plotted and acceptance criteria diagram overlaid, regions where the POD is above 95% confidence level can be indentified, meaning that we can see if the NDT system is accepted for a given application.

Two examples are given for the inspection of the copper lid: the change of the POD with the change of diameter of the FBH with fixed orientation, and the change of the POD with the change of the orientation of the FBH and fixed diameter, when the lid is inspected with available UT configurations.

As shown in Figure 5-11, at the time of the study the copper lid was inspected with totally six configurations. They have different setups, such as measurement direction, different technique (contact/immersion) and different focal laws.

Figure 5-12 shows the change of the volume POD for fixed angle and different diameters of the FBH across the cross section of the copper lid. The angle of the FBH is 90°, measured between the bottom of the FBH and a horizontal surface of the lid. Only UT configurations on the side surface of the lid will receive reflected sound wave from the FBH. The FBH with a diameter of 3 mm will have a high POD in the whole outer part of the lid. With decreasing diameter of the FBH, the POD is decreasing, with different rates in different regions. The rate of drop depends on how good the region is covered with UT configurations.

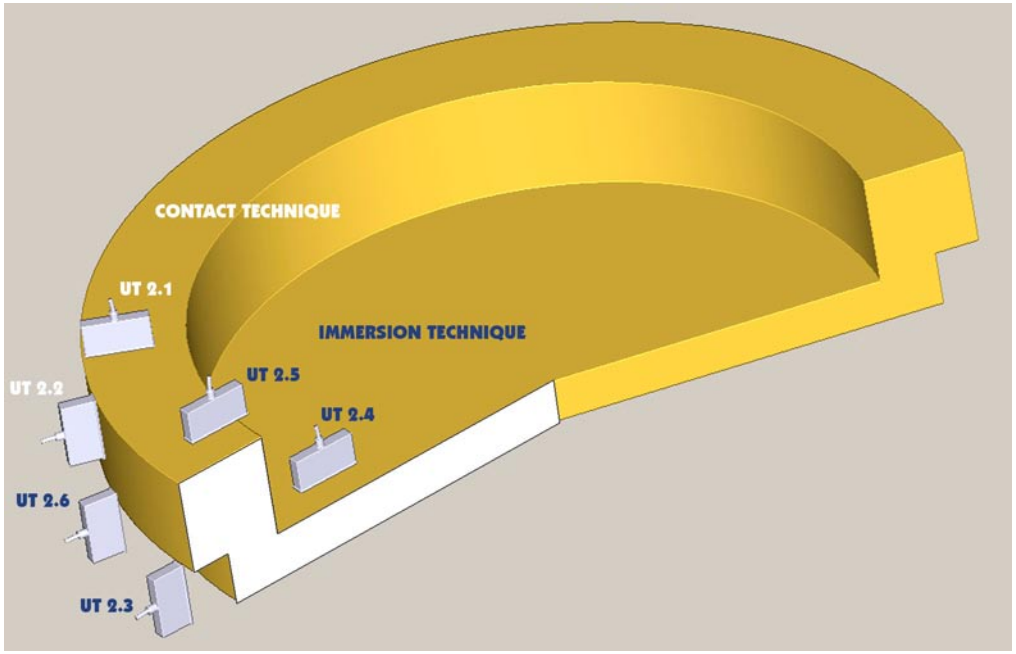

Figure 5-11. *Cross section of the lid with indicated UT configurations.*

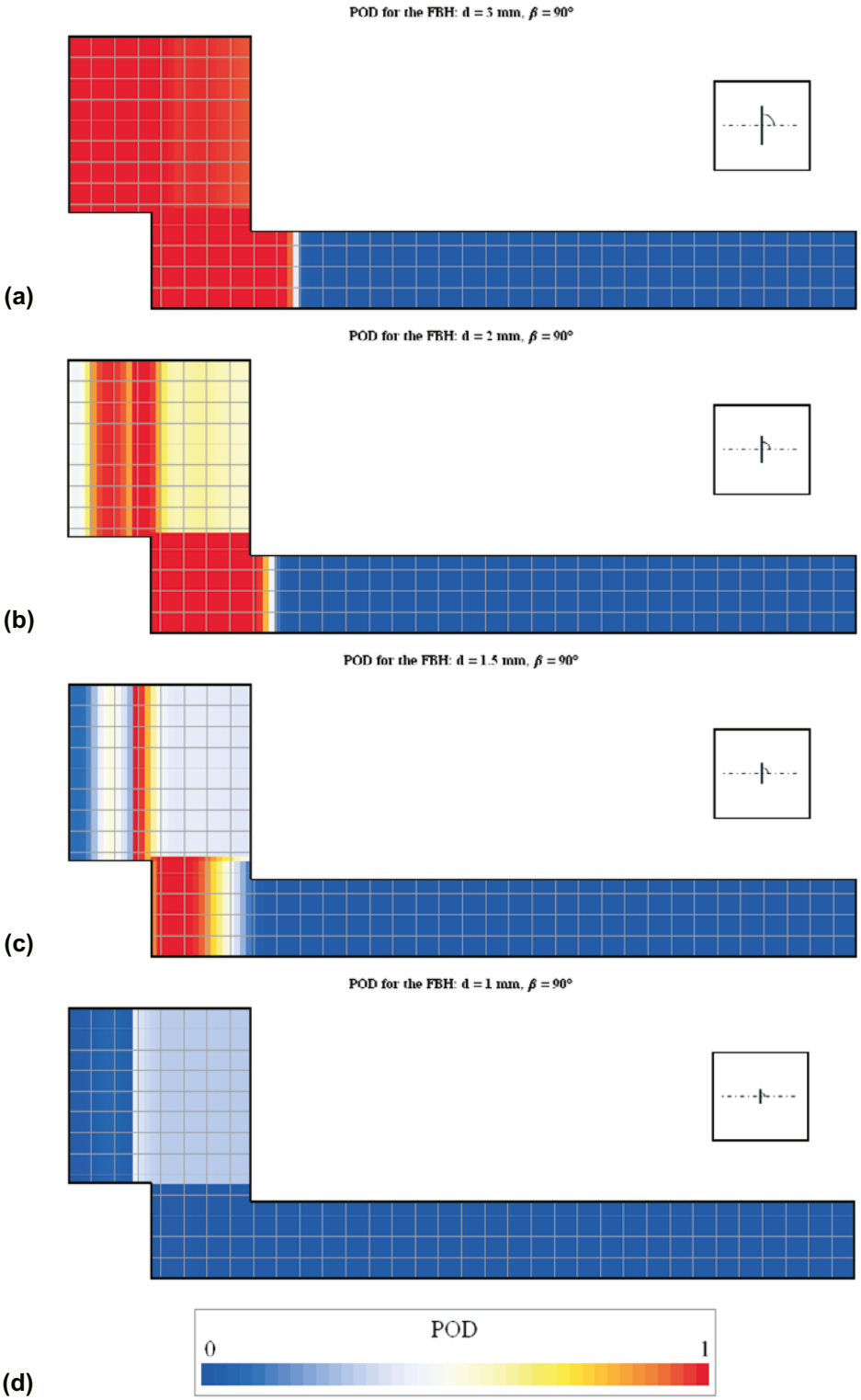

Figure 5-12. *The volume POD of the FBH with the diameters of (a) 3 mm, (b) 2 mm, (c) 1.5 mm and (d) 1 mm, all for orientation β = 90°. Small figures at the top right corner of the diagram show the orientation of the bottom surface of the analysed FBH.*

In Figure 5-13 the change of volume POD is shown when diameter of the FBH is held constant and the orientation of the FBH is changed. The FBH with orientation 0° (bottom of the FBH is parallel to the top surface of the lid) and diameter of 4 mm is shown first. Because of the horizontal orientation of the FBH, only UT configurations from the top surface of the lid will receive the reflected sound beam from the FBH. The POD is high across the whole cross section of the lid.

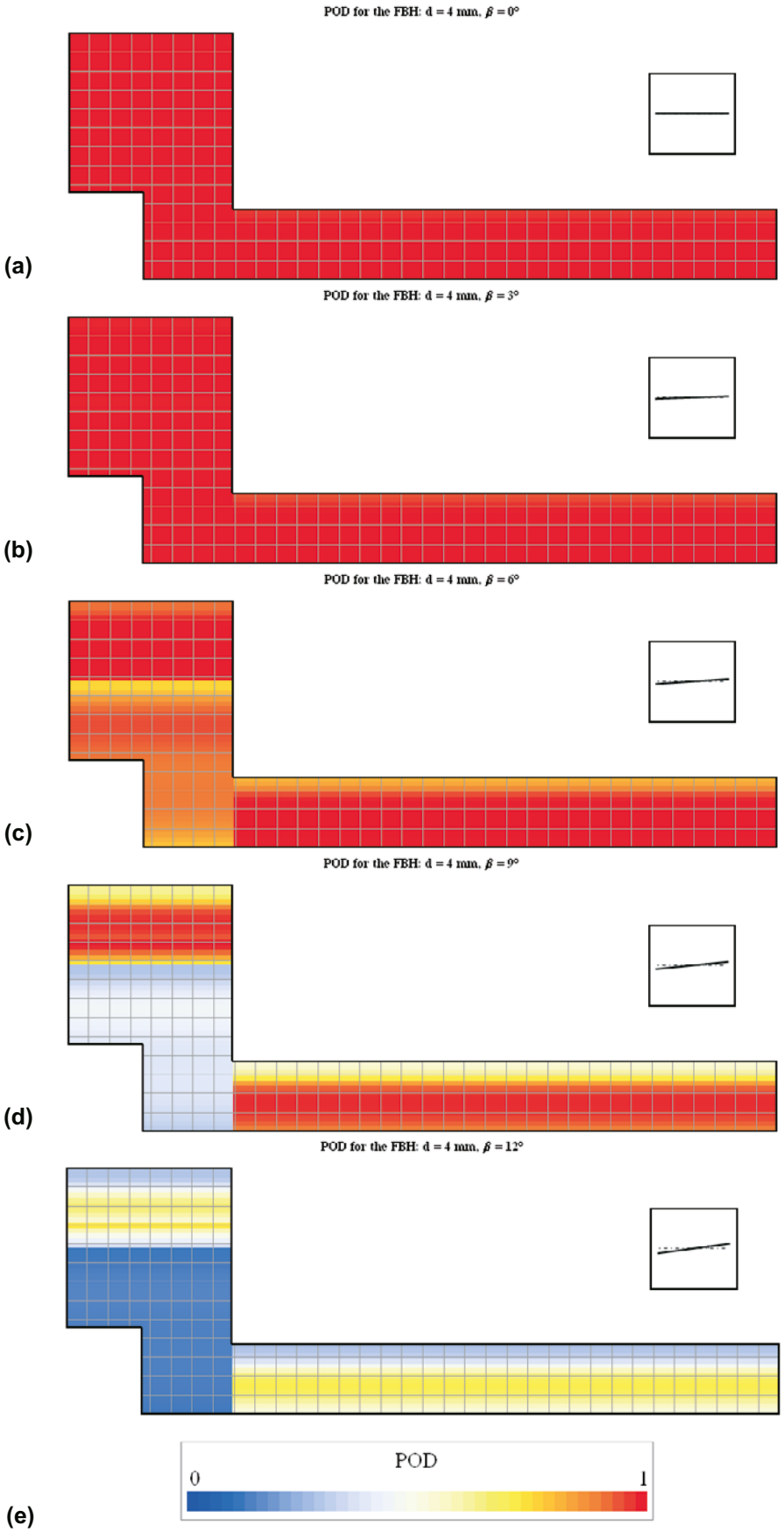

Figure 5-13. *Change of the volume POD for the FBH with the orientations of (a) 0°, (b) 3°, (c) 6°, (d) 9° and (e) 12°, all for diameter d = 4 mm. Small figures at the top right corner of the diagrams show the orientation of the bottom surface of the analysed FBH.*

With increasing angle, the POD is decreasing, again with different rates in different regions of the cross section. These rates are again dependent on the coverage of the region with UT configurations and on the individual POD's of the UT configurations.

If, instead of the POD, the region where the lower 95% confidence band is above 90% POD is indicated, it can be clearly identified whether the NDT system has sufficient reliability for the given task, as shown in Figure 5-14. Green regions indicate regions where the NDT system would be accepted for application. Non-green areas indicate that either additional UT configurations are needed to inspect the region or available UT configurations have to be optimized (to give higher POD).

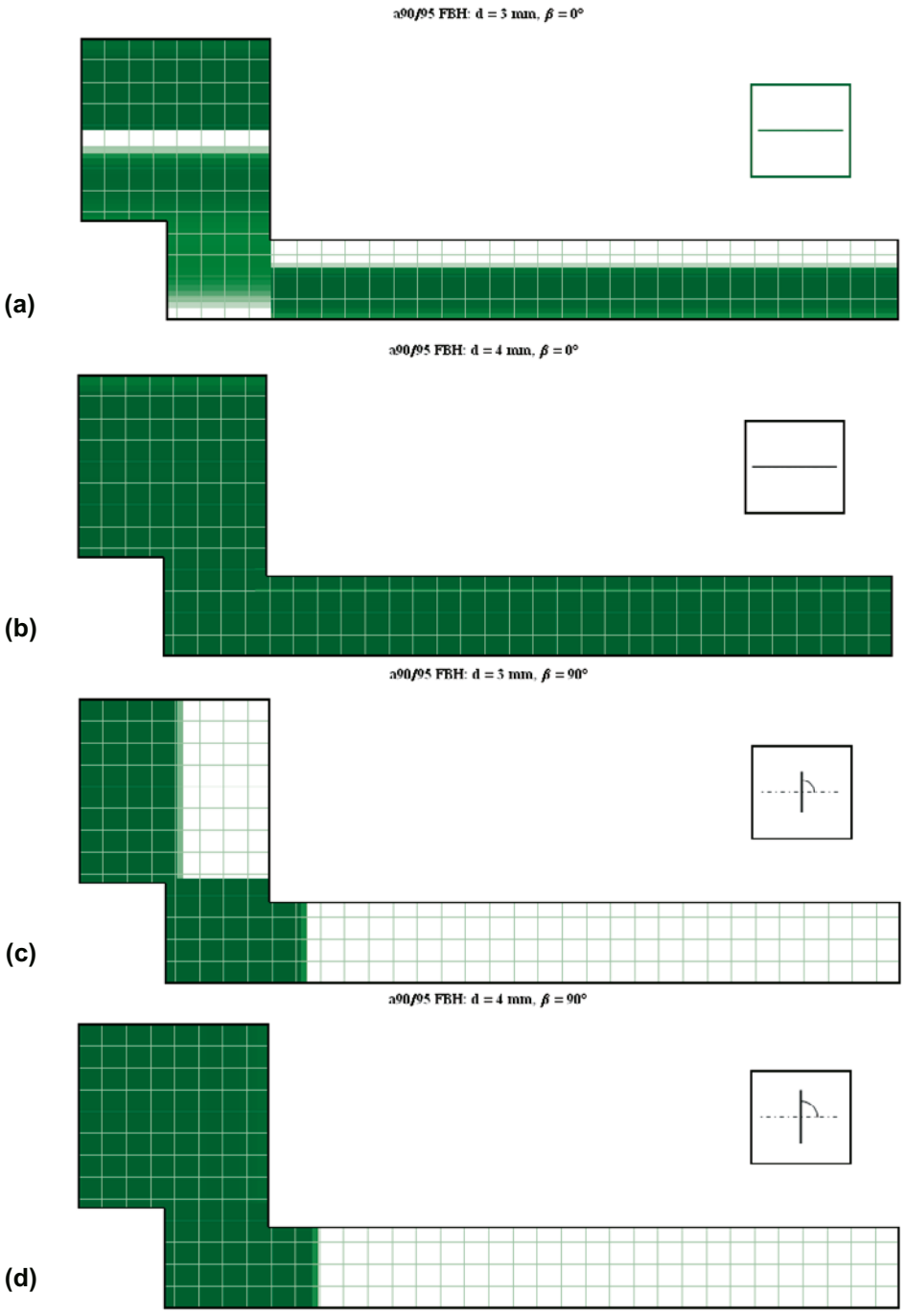

Figure 5-14. *Green regions of the cross section of the lid show where the lower 95% confidence band is higher then 90% POD for the FBH with diameters and orientations of (a) 3 mm and 0°, (b) 4 mm and 0°, (c) 3 mm and 90° and (d) 4 mm and 90°. Small figures at the top right corner of the diagrams show the orientation of the bottom surface of the analysed FBH.*

5.3 The POD II analysis

In conventional POD calculation with the $\hat{a}$ versus a analysis (also called signal response analysis), it is necessary to select a value, which represents the signal response of a defect as described in Section 5.1. An echo height (amplitude) in percent or signal-to-noise ratio of the reflection from a defect in a C-scan has been traditionally picked for this purpose. Defects must have a finite dimension so that the acquired reflection on a C-scan has a certain area in which the amplitude varies depending on the position, and the highest amplitude or the highest signal-to-noise ratio is normally selected for the calculation of the POD /6/.

The selection of a for FBH's or artificial defects is relatively simple, because of their simple shape, simple surface structure and large dimensions comparing to the size of the sound field. If the FBH surface is flat and normal to the incident angle, the maximum amplitude is located in the centre of the surface and amplitude distribution in the C-scan is the same as the sound field of the probe. However, in case of the real defects, it is difficult to select one value because real defects can have complicated shape and surface roughness, producing several local maxima in the C-scan. For example, the UT inspection of a real defect (wormhole in a weld) shown in Figure 5-15 creates a C-scan shown in Figure 5-16. The rough surface and the complicated shape of the defect respond irregularly creating many peeks in the C-scan as it can be seen in Figure 5-16. Although it is straightforward to select the highest peek and use it as the input value for the POD analysis, the value may not represent the characteristics of the defect. As a result, the peek value may produce larger scattering when plotted against a property of the defect (in the $\hat{a}$ versus a diagram) yielding in larger confidence bounds and in decrease of the $a_{90/95}$ value, i.e. the low reliability of the analysis.

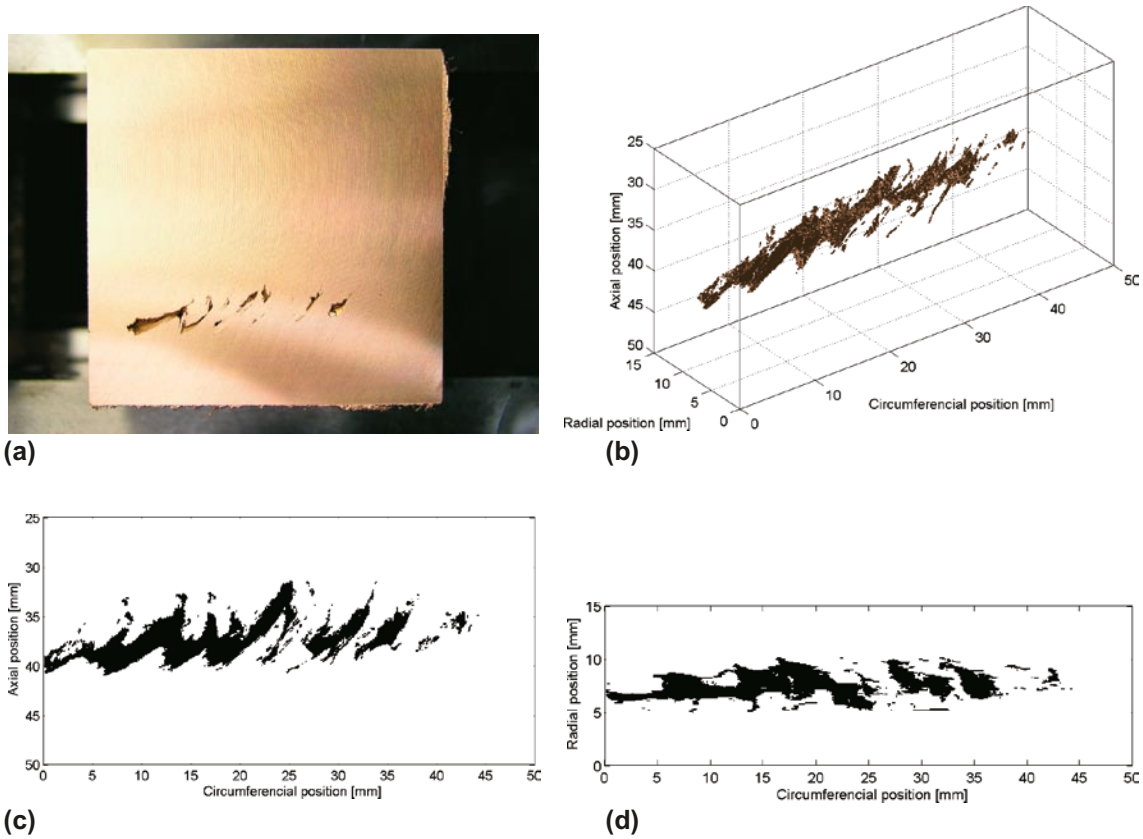

Figure 5-15. *Real defects found in a welded lid, FSW5, at 221°. (a) One of the pictures of the destructive sectioning at 7.0 mm from the outer perimeter. The dimension of the block is 50 × 50 mm. (b) Three-dimensional reconstructions of the defects from the destructive sectioning, (c) and (d) projections of the defects in radial direction and in axial direction, respectively.*

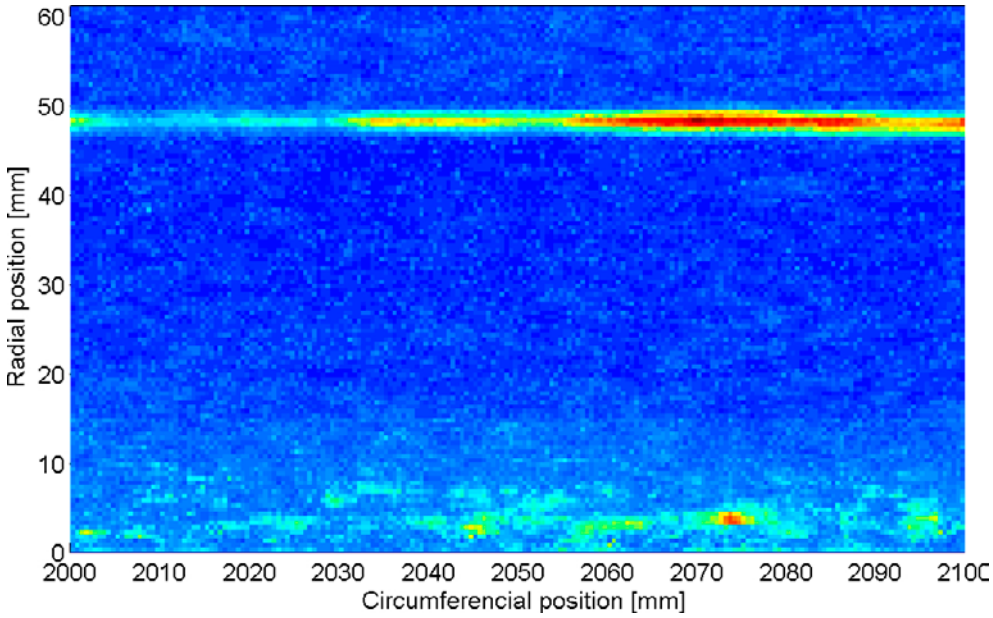

Figure 5-16. *Ultrasonic C-scan of the welded lid, FSW5. The data acquisition was performed from the top of the lid, i.e. in axial direction. The area shown in this figure corresponds to the area shown in Figure 5-15.*

A problem of the conventional approach mentioned above is to select a representative value for a defect from the data. This maximum value is not robust and can be influenced by many parameters, not only by the parameter to be analysed. Possible solutions are to take into account other influencing parameters as applied in POD I analysis, and/or to define another quantity than the highest amplitude as $\hat{a}$. The POD II analysis is exploring the possibilities of the second approach. The methodology and the results are described in this section.

5.3.1 Methodology

As mentioned in the previous section, the POD II analysis has been developed to pick another quantity than the highest amplitude as $\hat{a}$ for the conventional POD calculation with the signal response analysis. The new definition of the $\hat{a}$ must be more robust and must include more information than the conventional $\hat{a}$ in order to better represent the characteristics of the defect. One of the ideas of the approach is to use the spatial information of the reflectors. The method developed in this project exploits area/extent information. More specifically, the method utilizes the total amount of reflected amplitude from a defect as $\hat{a}$. The quantity can be calculated for each defect and it is easily imaginable that it depends directly on the area of a defect.

Definition of â

The ultrasonic testing equipment being used in the project employs a mechanized scanning as explained in Chapter 3. When the inspection is performed, a data set in three-dimensional volume is obtained and the C-scan is created from the data set. The quantity that is used as $\hat{a}$ in the method is defined by integration of amplitudes in the C-scan over a defect area as

$$\hat{a} := \int_S A(x, y)\, ds \tag{5-26}$$

where $A(x, y)$ is the amplitude distribution in the C-scan and S is the area of a defect. The calculation of the total amount of reflection amplitude would be more exact if the integration is performed in three dimensions (including the depth or time dimension), but for the simplicity, it is performed only in two, assuming that the pulse shape does not change with depth. In other words, frequency dispersion and frequency dependency of defect response are neglected.

By this definition, it is easily imaginable that the $\hat{a}$ is directly related to the area, which is illuminated by the sound field, i.e. the cross section of a defect in x-y plane. Therefore, areas of defect cross sections are taken as a in this method. Then, the same as in the conventional calculation of POD, it is assumed that the $\hat{a}$ is proportional to the a in logarithmic scale and the POD is calculated.

Threshold for the POD computation

A threshold needs to be set on an $\hat{a}$ versus a diagram when POD is computed. In the conventional POD calculation with the signal response analysis, the threshold is constant for a. The type of a constant threshold cannot be applied to the method proposed here, because a small defect detected with high reflection amplitude and a large defect with low amplitude may give the same level of POD if their $\hat{a}$ are of the same level. This is illustrated schematically in Figure 5-17. When there are two defects; a small one at a shallower depth (defect A) and large one at a larger depth (defect B), the amplitude profile of the C-scan should be like Figure 5-17(a), high amplitude and narrow distribution for A; and low and wide for B. In case that the areas for A and B in the amplitude profile (amplitude times width) are the same, the $\hat{a}$ for those two defects are the same and the $\hat{a}$ versus a diagram should be like Figure 5-17(b). Defects A and B have different cross sections but they have the same $\hat{a}$, so that the points are at the same level in the vertical axis. As described in Section 5.1, the POD is computed as integration of the estimated probability density function (PDF) from the threshold to the infinity, i.e. one minus the cumulative density function (CDF) at the threshold, thus the POD is basically defined by the vertical distance between those points and the threshold (shown by the dashed lines). Therefore, those two defects must have the same level of POD when a constant threshold (shown in the dashed-dotted line) is applied. However, in a real observation of a C-scan by human, it would be logical that the defect A has higher POD than the defect B, because A has a larger amplitude contrast to the surroundings.

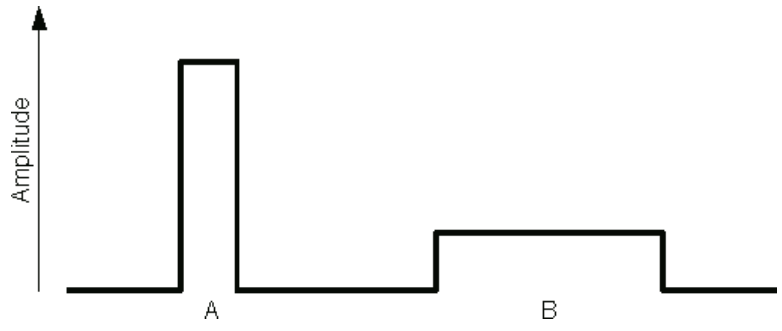

(a)

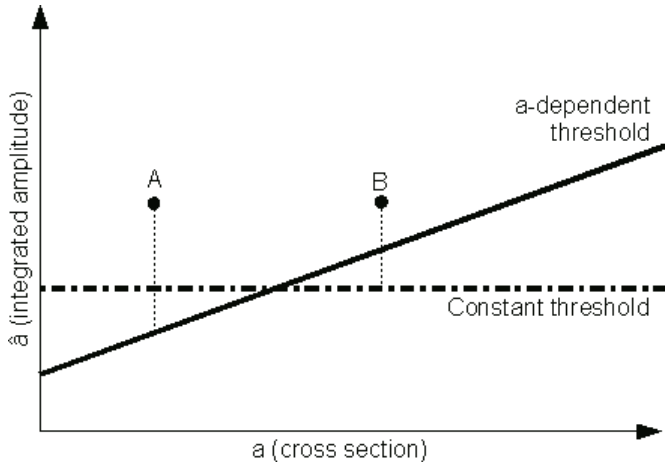

(b)

Figure 5-17. *Schematic illustration for an example of setting threshold. (a) Amplitude profile of a C-scan for a small defect at a shallower depth (defect A) and a large defect at a deeper depth (defect B). (b) The $\hat{a}$ versus a diagram of the defects in (a) and thresholds.*

It is also rather possible that $\hat{a}$ for a large defect exceeds the constant threshold by accumulating only noise although the defect does not appear in the C-scan at all, resulting the undetectable defect can have higher POD. In order to avoid those situations and to compute POD according to decision rules that inspectors are following in the observation process, an a-dependent threshold is proposed. The threshold is illustrated with the solid line in Figure 5-17(b) and it is linearly increasing with a (cross section in this case). By applying the threshold, distances to the points become longer for A and shorter for B as shown in Figure 5-17(b), resulting higher POD for A and lower POD for B. It is more similar to the decision making process of the observation of C-scans by human eyes.

5.3.2 Application and results of the method

The new POD analysis method developed above is demonstrated with an experimental data set. The data was acquired by the normal incidence, contact technique configuration for a test specimen of the copper lid. The top view of the test specimen is shown in Figure 5-18 and the obtained C-scan of the ultrasonic measurements is shown in Figure 5-19. Because of the too small width of the phased array probe, the entire body cannot be scanned at once so the data acquisition was performed in two steps, as it can be seen by two strips in the Figure 5-19. In this demonstration, the POD is calculated only for non-clustered FBH's. There are 14 such FBH's in the test body ranging from 2 to 8 mm in diameter and from 60 to 170 mm in depth.

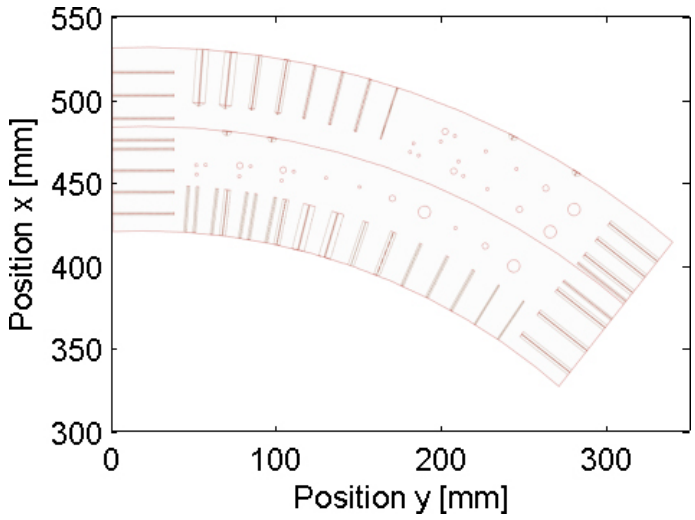

Figure 5-18. *Top view of the test specimen of the copper lid for the normal incidence, contact technique UT configuration. It has 14 FBH's excluding clustered ones.*

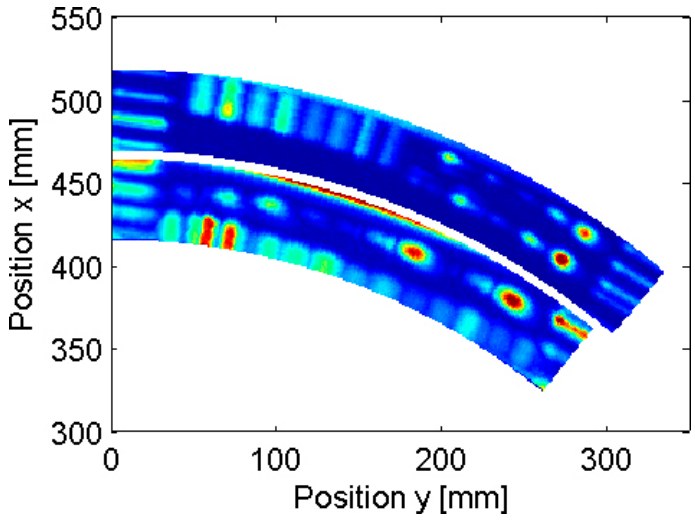

Figure 5-19. *Ultrasonic C-scan of the test specimen.*

Since these are laboratory measurements and the real dimensions of the defects are known, amplitudes directly above the area of FBH's can be extracted, as shown in Figure 5-20. The extracted amplitudes are integrated for each defect and they are plotted against the cross sections as an $\hat{a}$ versus a diagram shown in Figure 5-21(a). For a comparison, the conventional $\hat{a}$ versus a diagram is shown in Figure 5-21(b). The improvement of the fit compared to the conventional method cannot be clearly seen because the scales are different. But the confidence bounds (dashed lines) are slightly narrower in the new $\hat{a}$ versus a diagram, meaning that the quantity used as $\hat{a}$ is more stable than the conventional $\hat{a}$ although the measurements include errors.

As discussed in the previous section, a linearly increasing threshold T with a given by the following equation is applied.

$$T(a)=C_0+C_1\times NL\times\ln(a) \qquad (5\text{-}27)$$

where C_0 and C_1, and coefficients and NL is noise level taken from the C-scan. In the conventional POD analysis, we have chosen a constant threshold at three times higher than noise level. The decision threshold should be defined according to acceptance criteria; however it is not yet clearly defined and the both coefficients are set at 3. Therefore the slope of the a-dependent threshold applied is three times the noise level, which means that an average of the amplitudes within the area of a defect must be higher than three times noise level to exceed the threshold.

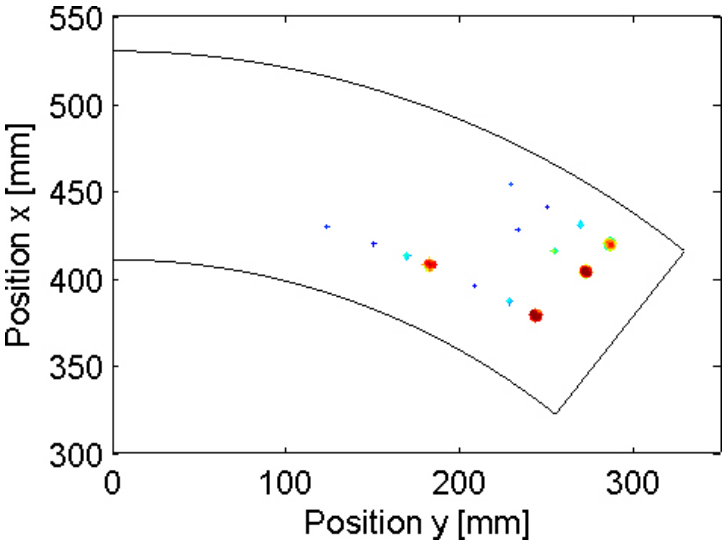

Figure 5-20. *Amplitudes in the C-scan at positions of the FBH's.*

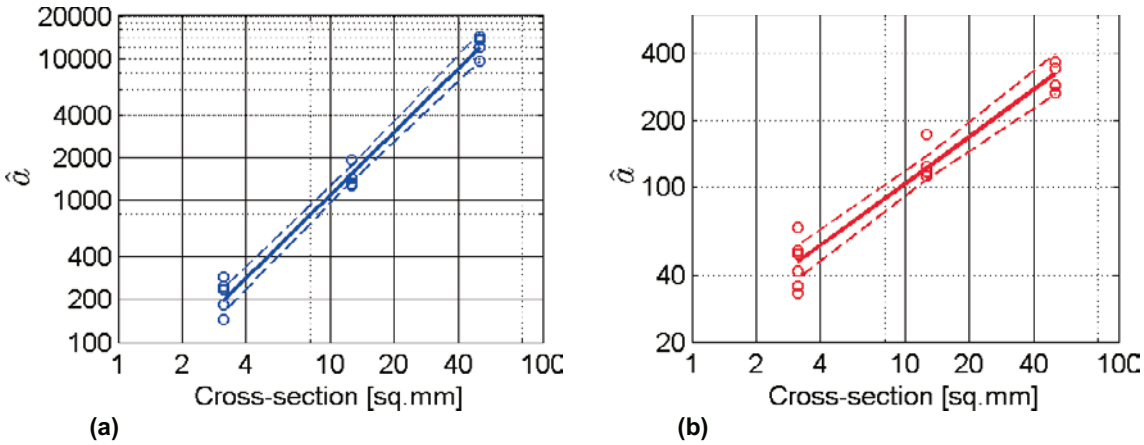

Figure 5-21. *â versus a diagrams with (a) newly defined â (integration of amplitudes), and (b) the conventional â (maximum amplitudes) in log-log scale. The solid and dashed lines show fitted lines to the measurements and the 95% confidence bounds, respectively.*

Figure 5-22 shows the POD curves calculated by the developed and the conventional methods. For the conventional POD curve, a constant threshold at the three times noise level is applied. Comparing those curves, the POD by the new method is higher. The reason may be that the new definition of $\hat{a}$ includes spatial information on the reflection. Although a defect is small or deep and it has low amplitudes, the C-scan for the defect has amplitude contrasts with a certain area corresponding to the real dimension of the defect if it is detectable. By integrating the amplitude over the area, the input quantity $\hat{a}$ for the POD calculation increases and thus the higher POD is obtained. For example, a FBH having a diameter of 2 mm, located at a depth of 140 mm has lower reflection amplitudes. The FBH gives POD's of 0.72 and 0.98 (at a cross section of 3.14 square mm) by the conventional and the new POD computation, respectively. The A-scan at a position where the maximum amplitude is given is shown in Figure 5-23. The highest amplitude (about 50% in amplitude, not in signal to noise ratio) is barely exceeding the decision threshold (indicated by the dashed-dotted line, about 40%). Considering the noise level (about 13%), FBH's of the same size can have amplitude lower than the threshold, resulting in lower POD.

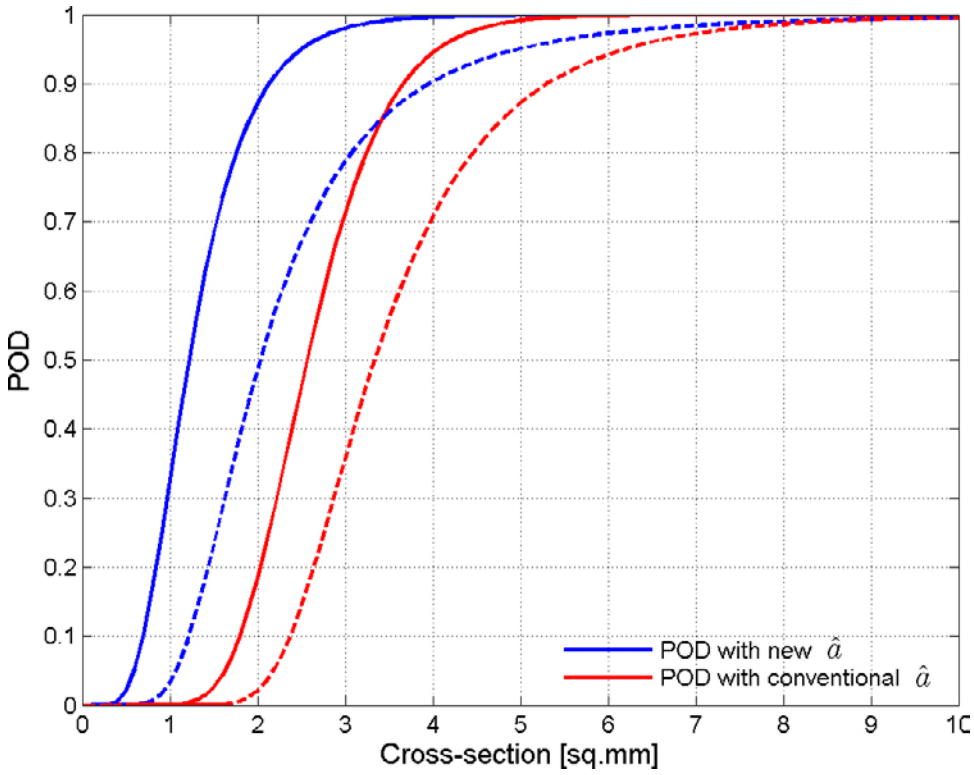

Figure 5-22. *POD curves calculated by the developed method (blue solid line) and the conventional method (red solid line) and the lower 95% confidence bounds (dashed lines).*

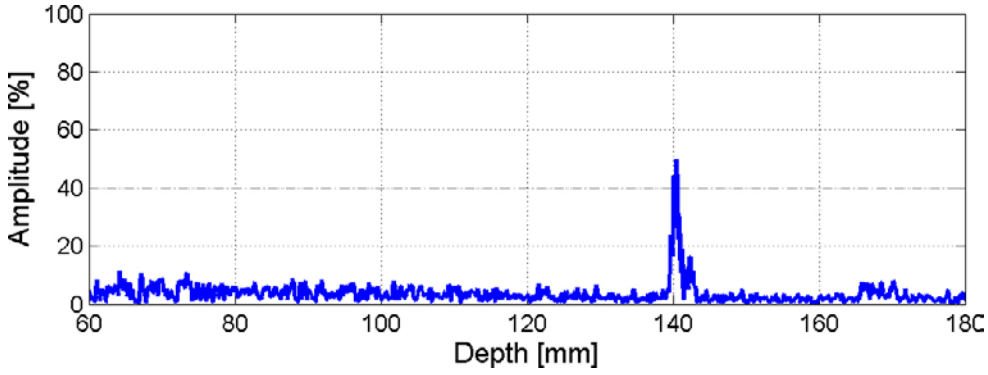

Figure 5-23. *A-scan for a FBH having a diameter of 2 mm at a depth of 140 mm. The dashed-dotted line shows decision threshold for the conventional POD calculation, which is set at three times the noise level.*

In the observation process of the ultrasonic data by the human inspector, the inspector checks a C-scan changing the contrast (colour scale) and looks for anomalies with certain areas or extents or shapes in most cases. In other words, human eyes look not only for higher amplitudes but also for distributions of those higher amplitudes. The C-scan for the same FBH (2 mm diameter, 140 mm depth) is shown in Figure 5-24. In this C-scan, the FBH is relatively easy to detect although amplitude values are low, because it has certain shape and contrast, which is different to noise pattern. Consequently, the POD for the FBH should be higher. The POD given by the new method is higher since it uses two-dimensional information. The new definitions of the $\hat{a}$ and the threshold are similar to the decision rules, which inspectors are applying, and thus the higher POD given by the new method can be seen as more realistic than in the conventional method.

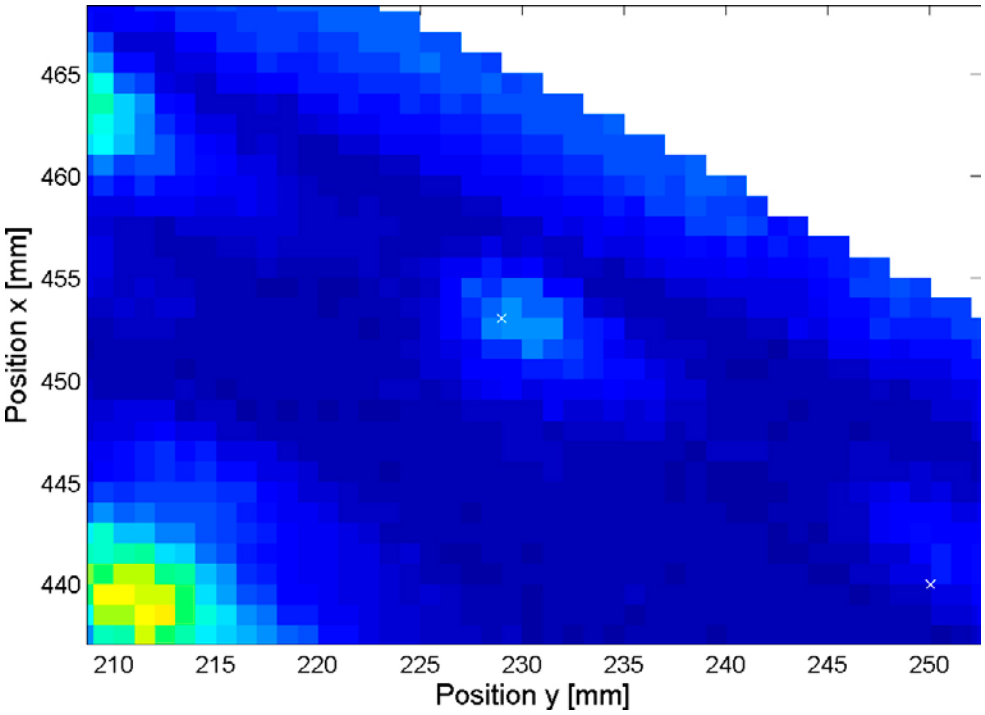

Figure 5-24. *C-scan at a FBH with a diameter of 2 mm at a depth of 140 mm indicated by the white cross at the centre of the figure.*

6 Conclusions

The details of the results of the reliability analysis of the UT phased array NDT system, used for the inspection of the canister components are published in the data reports for copper /9/ and cast iron /10/.

New methods developed in the course of the project, called the POD I and the POD II analysis, give better estimation of the reliability based on the better understanding of complex interaction between the sound field generated by the UT phased array system and the flaw. The UT configurations available for the inspection at the time of the analysis demonstrate good detection capability. Additional analysis will have to be performed when all of the planned UT configurations are available for the inspection. The UT system has to be tested against unfavourable positions of the flaws as well as locations to see if the whole volume of the canister is inspected with sufficiently high reliability.

6.1 Conclusions from the POD I analysis

The POD I analysis offers the unique opportunity to investigate the realistic, multi-parameter influence on the reliability of the NDT system. The results of the experiments clearly demonstrate that the response of the flaw to the UT phased array NDT system is dependent on more than only one parameter. Selected parameters, diameter, depth and orientation, have all large contribution to the reflection amplitude and therefore also influence on the detectability of the FBH. The quantity *a* is redefined as *multi-parameter a* to include those parameters with support of the modelling. Using modelling, other implicit influences on the amplitude are also taken into account, for example probe frequency and setup, wedge, focal laws, propagation velocity in material and so on. The resulting POD curve and its lower 95% confidence band plotted against the multi-parameter *a* (see Figure 5-6) are not easily physically interpretable, but they provide the opportunity to investigate the real, complex influences on the response. By varying only one parameter and fixing the others, the POD curve can be divided into POD curves for the single parameters (see Figure 5-7). This curve is similar to the conventional POD curve; however it reflects influences of the three parameters more accurately. For example, a POD curve with respect to depth and for a fixed diameter and angle of the FBH in Figure 5-7 (a) has a saddle which agrees with our knowledge about the shape of the sound field formed by the UT phased array probe. The more accurately calculated POD curve enables more thorough interpretation of the results. If the corresponding POD curve is calculated by the conventional method assuming linear relationship, the obtained POD curve would be a monotonic function, not reflecting the influence of the sound field form correctly. Therefore, applying the POD I analysis, the POD can be evaluated for each parameter more accurately what is a great advantage of the method. It is reasonable to expect that additional parameters also influence the detection and that they should also be included in the future analysis.

Multiple inspections of the same flaw with different UT configurations increase the total POD. The volume POD is able to combine and display POD's obtained from individual inspections. It is a way to display large amount of data from different inspections in a clear way and also a powerful tool which can serve not only as a final judgment of the goodness of the design of the NDT system but also as an optimisation tool. It is also appropriate way to display geometrical influences of the inspection object on the POD.

6.2 Conclusions from the POD II analysis

The POD II analysis developed in this project overcomes the limitations connected with the selection of the highest amplitude for $\hat{a}$ in the conventional POD analysis. A new definition of $\hat{a}$ as the integration of amplitudes over a defect area in the C-scan is proposed. The new $\hat{a}$ includes a piece of two-dimensional information by the integration. It contains more information and therefore it is more stable compared to the conventional method where the highest amplitude is selected as $\hat{a}$. Furthermore, a new decision threshold is proposed, which is linearly changing with a (for example, cross section of defects) in contrast to a constant threshold in the conventional $\hat{a}$ versus a analysis. The threshold is more similar to the decision rules that inspectors are actually applying when evaluating the data. As the result, those two new developments give higher POD than the conventional method. The higher POD can be seen as more realistic because the computation is more similar to the actual interpretation of the C-scan by inspectors.

The new developments incorporated in the POD II analysis presented in this report, have been applied only to the non-clustered FBH's. Since the FBH is one of the easiest targets, in order to see the effectiveness of the method it needs to be applied to the other types of artificial defects (such as SDH's and clustered FBH's) and on the real defects. It is an additional challenge for the POD II analysis.

6.3 ENIQ considerations

The POD I analysis shows the influence of variations of different parameters on the POD curve. In this report, the influence of variation of size, depth and orientation of the FBH was investigated. Including additional influencing parameters in the model, principally ENIQ parameters, we could observe their influence on the POD curve. Varying the parameters value and observing the influence on the POD, we could establish the range of values for selected parameter in which the NDT system still gives sufficiently high reliability (lower 95% confidence bound is higher than the 90% POD). This information would give us allowed deviation of the selected parameters which would still not endanger the function of the NDT system. The future investigation should be directed toward the selection of the essential parameters as prescribed by the ENIQ. These essential parameters for testing equipment, as for example ultrasonic equipment, manipulators, equipment for data evaluation, etc., have to be determined in an extensive form so that it is possible to make a qualified detection of all defects relevant for a quantitative POD after having changed the testing equipment. The changed equipment has to fulfil the same essential parameters and conditions as the equipment used for qualification. The essential parameters are categorised as follows:

1. Component parameters.
2. Defect parameters.
3. Procedure parameters.
4. Equipment parameters.
5. Technical parameters.

A pre-selection of parameters, their inclusion in the model calculation and investigation of their influence on the POD as well as the determination of the range of the values of parameters which still results in acceptable NDT system is the subject of the future work.

7 References

/1/ **SKB, 2007.** RD&D Programme 2007. Programme for research, development and demonstration of methods for the management and disposal of nuclear waste. SKB TR-07-12, Svensk Kärnbränslehantering AB.

/2/ **SKB, 2006.** Long-term safety for KBS-3 repositories at Forsmark and Laxemar – a first evaluation, Main report of the SR-Can project. SKB TR-04-11, Svensk Kärnbränslehantering AB.

/3/ **Meeker W Q, Escobar L A, 1998.** Statistical methods for reliability data. Wiley, New York.

/4/ **US Department of Defense, 1999.** Nondestructive Evaluation System – Reliability Assessment, MIL-HDBK-1823.

/5/ **European Commission Joint Research Centre, 2007.** European methodology for qualification of non-destructive testing – Third issue, ENIQ Report No. 31, EUR22906EN.

/6/ **Berens A P, 1989.** NDE Reliability Data Analysis – Metals Handbook, Volume 17, 9th Edition: Nondestructive Evaluation and Quality Control, ASM International, OH.

/7/ **Müller C, Elagin M, Scharmach M, Bellon C, Jaenisch G R, Bär S, Redmer B, Geobbels J, Ewert U, Zscherpel U, Boehm R, Brekow G, Erhard A, Heckel T, Tessaro U, Tscharntke D, Ronneteg U, 2006.** Reliability of nondestructive testing (NDT) of the copper canister seal weld. SKB R-06-08, Svensk Kärnbränslehantering AB.

/8/ **Ronneteg U, Cederqvist L, Rydén H, Öberg T, Müller C, 2006.** Reliability in sealing of canister for spent nuclear fuel. SKB R-06-26, Svensk Kärnbränslehantering AB.

/9/ **Pavlovic M, Takahashi K. Müller C, 2008.** NDT Reliability – data report copper, SKBDoc. id 1180131.

/10/ **Pavlovic M, Takahashi K, Müller C, 2008.** NDT Reliability – data report insert, SKBDoc. id 1180132.

/11/ **Boehm R, Wüstenberg H, Erhard A, Brekow G, Tessaro U, 2001.** Überlegungen zur Fehlergrößenbestimmung bei rissartigen Fehlern im Plattierungsbereich mit TOFD, in Proc. DGZfP-Jahrestagung 2001, Berlin.

/12/ **Boehm R, Ehard A, Wüstenberg H, Rehfeldt T, 2002.** Dreidimensionale Berechnung von Schallfeldern unter dem Einfluss zylindrischer Bauteilkrümmungen für fokussierende Prüfköpfe und Gruppenstrahler, in Proc. DGZfP-Jahrestagung 2002, Weimar.

/13/ **Boehm R, Erhard A, Rehfeldt T, 2003.** Einfluss fokussierter Schallfelder auf das Reflexionsverhalten von Testfehlern, in Proc. DGZfP-Jahrestagung 2003, Mainz.

/14/ **Boehm R, Erhard A, 2004.** Simulationsgestützte Entwicklung von Ultraschallprüfköpfen, in Proc. DACH-Jahrestagung 2004, Salzburg.

/15/ **Boehm R, Erhard A, Rehfeldt T, 2004.** Reflexionsverhalten in fokussierten Schallfeldern, MP Materials Testing, Issue 01–02, pp. 46–52.

/16/ **Boehm R, Erhard A, Vierke J, 2005.** Anwendung von Modellen zur Echohöhenbewertung von Prüfköpfen mit ungewöhnlicher Schwingergeometrie, in Proc. DGZfP-Jahrestagung 2005, Rostock.

/17/ **Tscharnke T, Boehm R, Erhard A, Müller C, Ronneteg U, Rydén H, 2006.** Ultrasonic investigations on copper canister welds in preparation for the storage of spent nuclear fuel in a deep repository, in Proc. 9th European Conf. NDT, Berlin.

/18/ **Boehm R, Erhard A, 2006.** Modelling of reflectivity patters from artificial defects, in Proc. 9th European Conf. NDT, Berlin.

/19/ **Boehm R, Spruch W, 2006.** Phased array rotation scanner probe system for ultrasonic testing of sleeve shafts, in Proc. 9th European Conf. NDT, Berlin.

/20/ **Spies M, 1994.** Transducer-modeling in general transversely isotropic media via point-source synthesis: theory, J. Nondestr. Eval., Vol. 13, No. 2, pp. 85–99.

/21/ **Cheng R C H, Iles T C, 1983.** Confidence bands for cumulative distribution functions of continuous random variables, Technometrics, Vol. 25, No. 1, pp. 77–86.

/22/ **Cheng R C H, Iles T C, 1988.** One sided confidence bands for cumulative distribution functions, Technometrics, Vol 32, No 2, pp. 155–159.

/23/ **European Commission Joint Research Centre, 2005.** ENIQ recommended practice 1 – Influential/essential parameters (Issue 2), ENIQ Report No. 24, EUR21751EN.